





MASTER

Engineering and International Space Law in Communications, Navigation and Sensing Satellite Systems

COMPARISON OF TOTAL COLUMN OZONE VALUES COLLECTED ON BOARD SATELLITE BY THE TOTAL OZONE MAPPING SPECTROMETER - EARTH PROBE (TOMS-EP) AND BY THE OZONE MONITORING INSTRUMENT (OMI) - AURA WITH DATA COLLECTED AT GROUND BY THE BREWER SPECTROPHOTOMETER LOCATED AT THE AIR FORCE - TECHNICAL CENTRE FOR METEOROLOGY (CTM).

Supervisors Author

Prof. Ernestina CIANCA Lt. Colonel GArn Alessandro GALLIANI

General Inspector GArn Silvio CAU

Contents

Preface		ii
Chapter 1	Ozone in the Atmosphere	1
1.1	Objectives	1
1.2	Ozone	1
1.3	The ozone formation, a simple model	3
1.4	Ozone measurement and UV radiation	6
Chapter 2	The measurement of total ozone aboard satellite	9
2.1	Objectives	9
2.2	The Total Ozone Mapping Spectrometer TOMS	9
2.3	The Ozone Monitoring Instrument (OMI)	14
Chapter 3	The measurement of total ozone at ground	21
3.1	Objectives	21
3.2	The BREWER Spectrophotometer	21
3.3	Spectrophotometer	22
3.4	Solar tracking system	26
3.5	Personal Computer operating Software	27
3.6	Processing algorithm for total column ozone	27
3.7	The Italian Air Force BREWER of Vigna di Valle	30
Chapter 4	Comparison between satellite and ground total ozone column measurements	31
4.1	Objectives	31
4.2	Comparing TOMS – BREWER data	31
4.3	Comparing OMI – BREWER data	36
4.4	Conclusions	39
Bibliography		40

Preface

Ozone is one of the most important trace gases in our atmosphere. The peak concentration of ozone in the atmosphere is in the stratosphere, where the ozone layer acts as a "sunscreen" for human beings by shielding the Earth's surface from harmful ultraviolet radiation. This absorption of solar energy also affects atmospheric circulation patterns and thus influences weather worldwide. In addition, ozone absorbs infrared radiation, and is a most powerful greenhouse gas in the cold upper troposphere located 8–15 km above the surface. Moreover, throughout the atmosphere, ozone is the key element fuzing chemical cleansing of the atmosphere from various pollutants, such as carbon monoxide and methane, among others, which could otherwise accumulate to harmful levels or exert a stronger influence on climate. High ground-level ozone amounts contribute to poor air quality, adversely affecting human health, agricultural productivity, and forested ecosystems. Therefore, changes to ozone distribution in the atmosphere as a whole can have major impacts on the Earth and for this reason ozone is measured throughout the atmosphere with instruments on the ground, airborne, on high-altitude balloons, and spaceborne. The purpose of this work is to compare the total column ozone values obtained by instruments on board satellite Total Ozone Mapping Spectrometer – Earth Probe (TOMS-EP) and Ozone Measurement Instrument (OMI) – AURA with the ground values obtained by the Brewer Spectrophotometer located at the Italian Air Force Technical Centre for Meteorology (CTM). In the first chapter is described what ozone is. The ozone concentration and its mean distribution as a function of latitude and seasons are showed. A simple atmospheric ozone formation model based on photochemical reactions is described and the transport mechanism due to the general atmospheric circulation is showed. Finally, the importance of measuring ozone due to its property to absorb the ultraviolet radiation (UV) emitted by the Sun is illustrated. The second and the third chapter show how total ozone measurements respectively aboard satellite and at ground are done. In detail, the second chapter describes how the Total Ozone Mapping Spectrometer (TOMS) and the Ozone Monitoring Instrument (OMI) operate aboard satellite. The third chapter describes how the Brewer spectrophotometer operates at ground. In the last chapter the comparison between collected total ozone column values at ground and on board satellite is showed. Data collected on board satellite are compared with those measured at ground by means of a statistical analysis. The results of the comparison between TOMS and BREWER data in the period from January 1998 to January 2009 and between OMI and BREWER data in the period from September 2015 to September 2020 are presented. In both cases satellite and ground measurements are very similar and in good agreement.

Chapter 1

OZONE IN THE ATMOSPHERE

1.1 – Objectives

This chapter describes what the ozone is. The ozone concentration in the atmosphere and its mean distribution as a function of latitude and seasons are showed. A simple atmospheric ozone formation model based on photochemical reactions is described and the transport mechanism due to the general atmospheric circulation is showed. Finally, the importance of measuring ozone due to its property to absorb the ultraviolet radiation (UV) emitted by the Sun is illustrated.

1.2 - Ozone

Ozone, whose chemical formula is O₃, is a naturally occurring substance which was first made in the laboratory in 1839 by German scientist Christian Friedrich Schönbein. The scientist was interested in discovering the origin of the odour produced by certain chemical and electrical processes. Although the first measurements were carried out in Arosa (Switzerland) and Oxford (England) in 1920, only at the end of 1950s a measurement network for ozone monitoring was established. Measurements of solar radiation, whose output peak is about 550 nm, showed that the radiation sent out from its surface, reaching the Earth's surface, is generally consistent with the spectrum of a black body with a temperature in the range of 5.500 – 6.000 K, but without any radiation below a wavelength of about 310 nm at the ultraviolet end of the spectrum (Figure 1.1). The missing radiation was being absorbed by something in the atmosphere. Did not take long before scientists found ozone to be the responsible absorbing element. Measurements of the solar spectrum were later used to estimate the amount of ozone in the path between the sun and the ground. Ozone is one of the most important trace gases in our atmosphere. High ground-level ozone amounts contribute to poor air quality, adversely affecting human health, agricultural productivity, and forested ecosystems. In addition ozone absorbs infrared radiation, and is most potent as a greenhouse gas in the cold upper troposphere located 8–15 km above the surface. We now know the peak concentration of ozone in the atmosphere is in the stratosphere, the atmospheric region approximately between 15 and 50 km of height (Figure 1.2). In the stratosphere the ozone layer acts as a "sunscreen" for human beings by shielding the Earth's surface from harmful ultraviolet radiation. This absorption of solar energy also affects atmospheric circulation patterns and thus influences weather worldwide. Moreover, throughout the atmosphere, ozone is the key ingredient that initiates chemical cleansing of the atmosphere of various pollutants, such as carbon monoxide and methane, among others, which could otherwise accumulate to harmful levels or exert a stronger influence on climate. Therefore, changes to ozone anywhere in the atmosphere can have major impacts on the Earth. If all the ozone molecules in a column of the atmosphere at middle latitudes were separated out from the rest of the air molecules and compressed to standard temperature and pressure (STP, equal to 0 °C and 1 atmosphere surface pressure), the resultant column of ozone would be only about 3 mm thick (about 1 molecule in a million of air). The measured column of ozone is generally reported as a length unit. The 'milli-atmo-centimetre' at STP, historically the standard unit of ozone, has been named the Dobson Unit (DU) in honour of Gordon M.B. Dobson, the first scientist to make large-scale, systematic measurements of ozone. One Dobson Unit is also equivalent to 2.68 × 10 ²⁰ molecules·m ⁻². Photochemical reactions occurring in the stratosphere above the equator produce the ozone. A slow, global-scale mixing of air called the Brewer-Dobson circulation (Figure 1.3) rises tropospheric air into the stratosphere in the Tropics and moves ozone poleward. Ozone descends in the high latitudes and is is destroyed by other photochemical reactions. At mid-latitudes, ozone could be considered a trace gas.

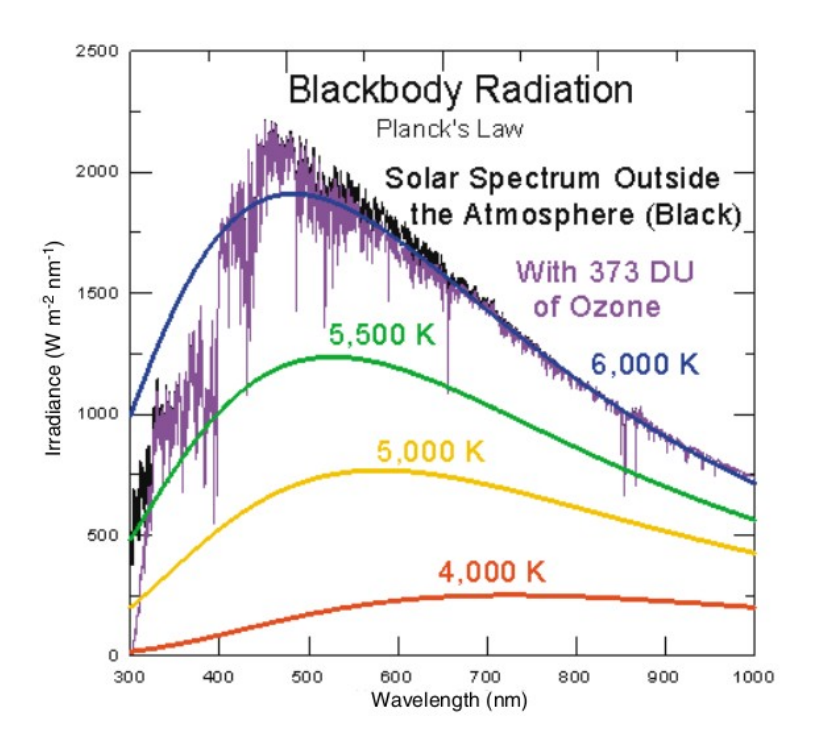


Figure 1.1 - Solar spectrum with (purple) and without (black) ozone absorption from a path of 373 DU of ozone. - (Courtesy of C.T. McElroy and P.F. Fogal, 2007).

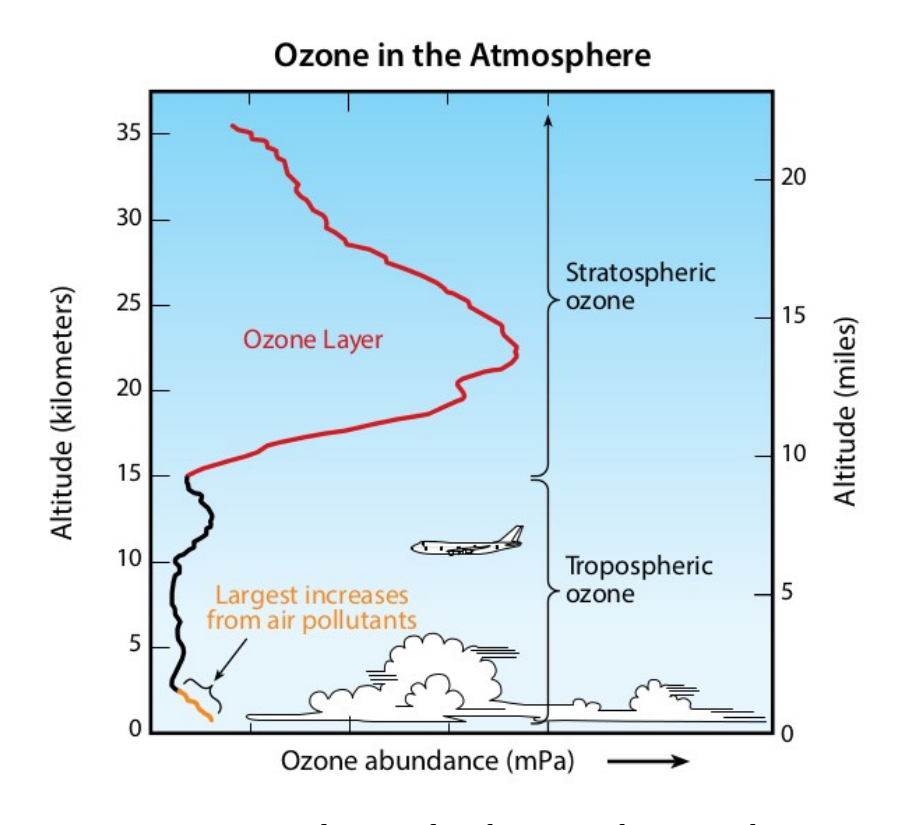


Figure 1.2 – Vertical ozone distribution in the atmosphere. (Courtesy of R.J Salawitch and coauthors, 2018)

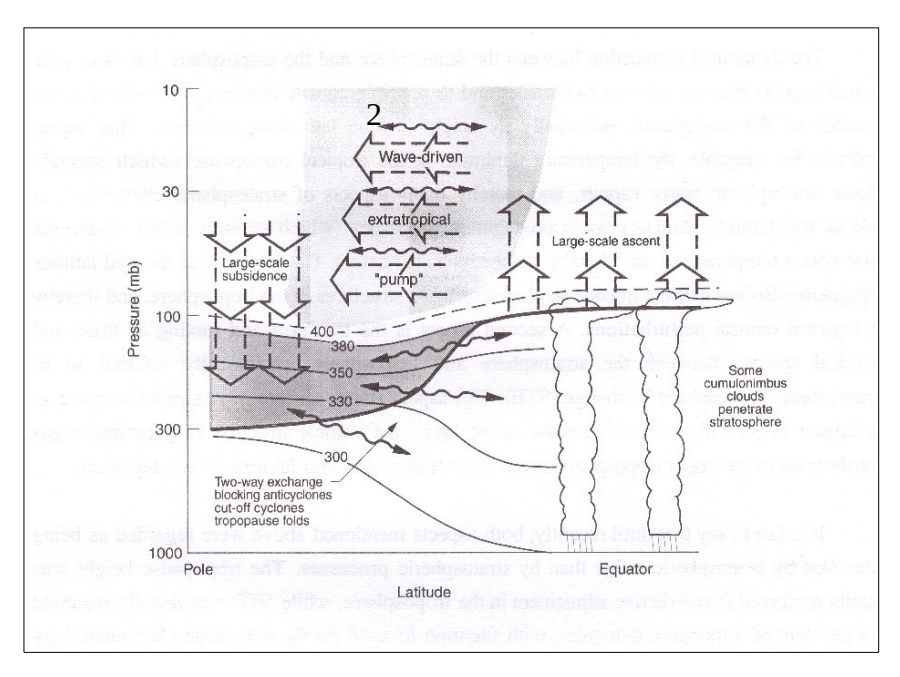


Figure 1.3 – Brewer – Dobson circulation. (Courtesy of Holton,1995)

1.3 The ozone formation, a simple model.

Ozone has the ability to absorb UV radiation. In figure 1.4 the absorption cross section for ozone in the range 200-850 nm is showed. Ozone strongly absorbs in the UV range 200-310 nm (Hartley band) and weakly in the UV range 310-350 nm (Huggins band). Absorption bands are also present in the visible range 400-850 nm (Chappuis bands).

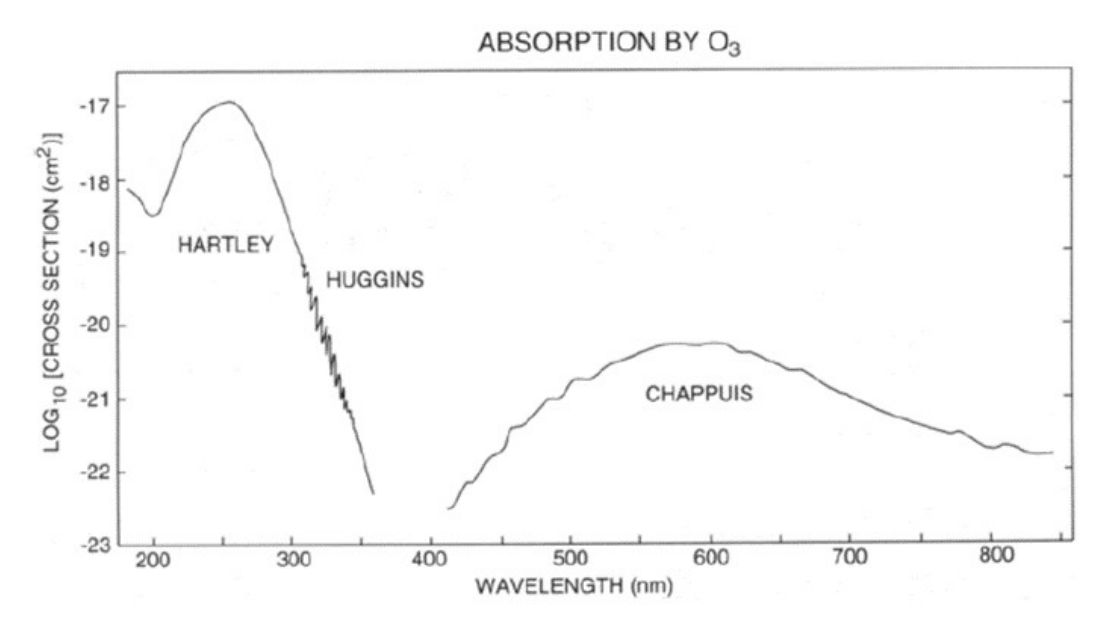


Figura 1.4 – Absorption cross section for ozone. (Courtesy of M.L. Salby, 1996)

Sydney Chapman in 1927 proposed a cycle of chemical reactions driven by the Sun as the mechanism for sustaining it. The elementary model is based on the assumption that the atmosphere is formed only by oxygen.

The ozone is created when oxygen atoms and oxygen molecules combine as in the following:

• Molecular oxygen dissociation forms atomic oxygen:

$$O_2 + hv \rightarrow^{J_1} O + O$$
 ($\lambda < 242,4 \text{ nm}$) (1.1)

where J is the photodissociation rate.

• Atomic oxygen combines with molecular oxygen to produce ozone:

$$O + O_2 + M \Rightarrow^{k_1} O_2 + M + 24 kcal \cdot mol^{-1}$$

$$\tag{1.2}$$

where K is the reaction coefficient representing the formation rate and M is a background inert gas which absorbs the excess energy produced by the process. In the atmosphere M is the molecular nitrogen.

The ozone is destroyed and atomic oxygen and molecular oxygen are formed as in the following:

• Ozone dissociation:

$$O_3 + hv \rightarrow^{J_2} O + O_2$$
 ($\lambda < 1134,4 \text{ nm}$) (1.3)

$$O_3 + O \rightarrow^{k_2} O_2 + O_2 + 94 \ kcal \cdot mol^{-1}$$
 (1.4)

In addition a three bodies combination reaction is present:

$$O + O + M \rightarrow^{k_2} O_2 + M + 118 kcal \cdot mo\Gamma^{-1}$$

$$\tag{1.5}$$

If n_1,n_2,n_3 are the numeric density of O, O_2 , O_3 in the atmosphere at a height z and at a time t and n_M is the background gas concentration, the variation of the densities is represented by the following equations systems:

$$\begin{vmatrix} \frac{\partial n_1}{\partial t} = 2J_1 n_2 + J_2 n_3 - 2K_3 n_M n_1^2 - K_1 n_M n_1 n_2 - K_2 n_1 n_3 \\ \frac{\partial n_2}{\partial t} = -J_1 n_2 + J_2 n_3 + K_3 n_M n_1 - K_1 n_M n_1 n_2 + 2K_2 n_1 n_3 \\ \frac{\partial n_3}{\partial t} = -J_2 n_3 + K_1 n_M n_1 n_2 - K_2 n_1 n_3 \end{vmatrix}$$
(1.6)

If we assume n_M is the nitrogen molecules concentration and the transportation due to the atmosphere is not considered, it is possible cancel the dependence on n_M using the following equation:

$$0.5 \cdot n_T(z) = 0.21 \cdot n_M(z) \tag{1.7}$$

where the total numeric density is $n_T = n_1 + n_2 + n_3$

Introducing (1.7) in (1.6) the variables $n_1(z,t)$, $n_2(z,t)$, $n_3(z,t)$, depend on the photodissociation rate and the reaction coefficients. With the further hypothesis that the photodissociation and reaction coefficients are independent on the concentrations, if we know the initial values of the concentration and their dependence on z, the linear equation system becomes a three variable system, the variables are only a function of z and the system can be solved. If the photochemical equilibrium is reached the equation system becomes an algebraic system.

Figure 1.5 shows the stratospheric ozone and oxygen concentration. While the shape of the distribution is coherent with observations, because a maximum in the ozone concentration is present at about 30 km, the peak concentration is rather high in value.

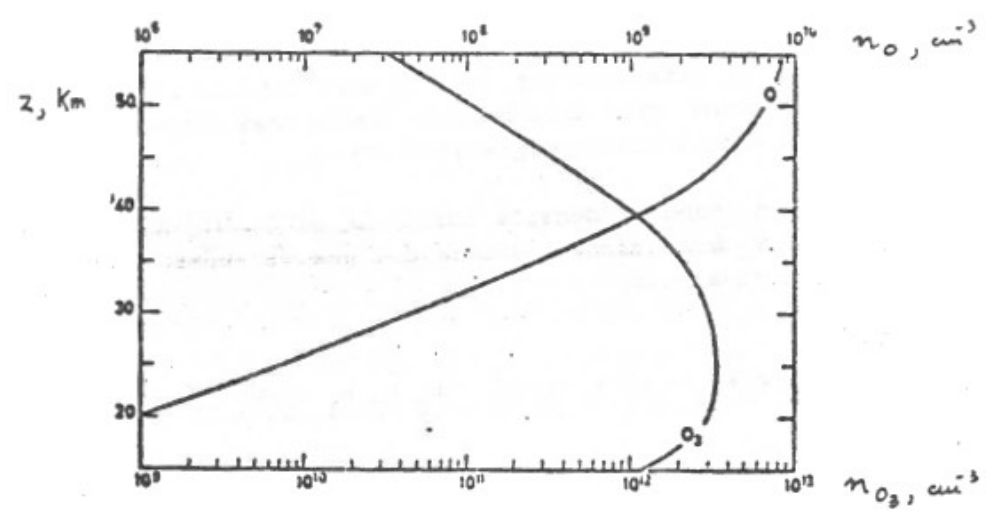


Figure 1.5 - Stratospheric ozone and oxygen concentration. (Courtesy of G. Fiocco, 1986)

Photochemical reactions and BREWER - Dobson circulation act together. Once the air has descended, outside the tropics, the short wavelength light needed to break up oxygen molecules is no longer available and there is no net production of ozone. Photochemical reactions of ozone produces oxygen atoms, but most of these immediately rejoin oxygen molecules and thus turn back into ozone. This cycle provides a net input of energy to the upper atmosphere, creating the temperature inversion that characterize the stratosphere.

The distribution of total ozone over Earth varies with location on timescales ranging from daily to seasonal. The variations are caused by large-scale movements of stratospheric air and the chemical production and destruction of ozone. Total ozone content is generally lowest at the equator and highest in polar regions. In polar regions there are a number of reactions producing a steady destruction of ozone compensated for, in terms of the total column ozone content, by the air descent, resulting in a thicker ozone layer, and the nearly constant mixing ratio results in a higher concentration of ozone in molecules per volume unit. This descent, as the air moves poleward, that leads to the maximum of ozone content at higher latitudes in late winter and early spring. It also causes the peak in the ozone profile to descend toward the poles outside of the subtropics. The mean ozone distribution as a function of latitude and seasons is showed in figure 1.6.

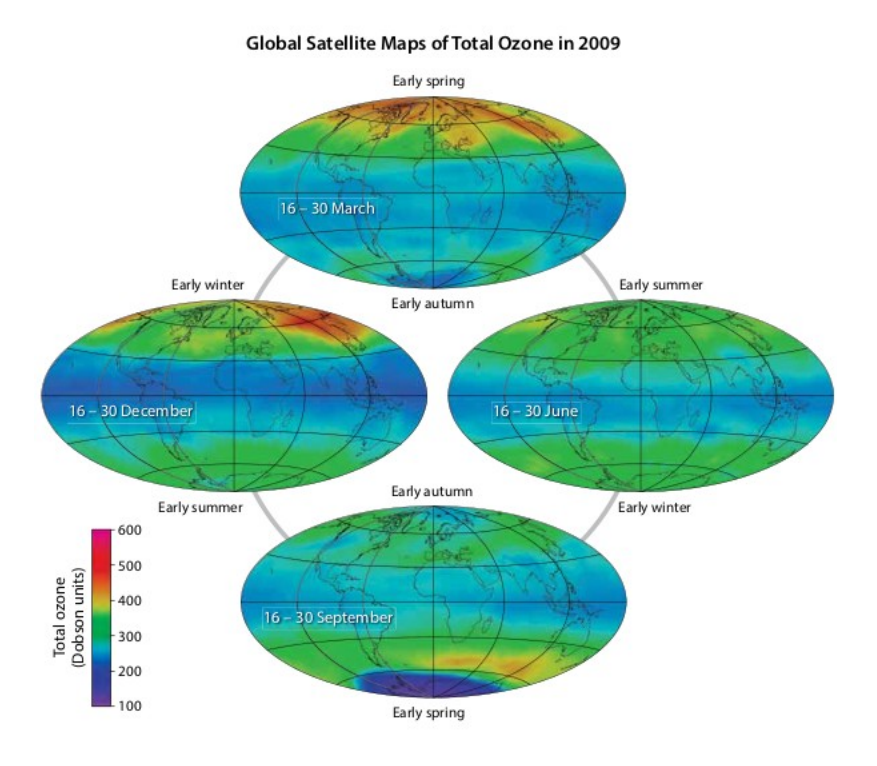


Figure 1.6 – Mean ozone distribution as a function of latitude and season. (Courtesy of R.J Salawitch and coauthors, 2018).

1.4 Ozone measurement and UV radiation

Radiation from the Sun includes light, heat and UV radiation. The UV region of the spectrum (figure 1.7) covers the wavelength range 100–400 nm for which human eye has no normal visual response. UV is divided into three bands: UVA (315–400 nm), UVB (280–315 nm), UVC (100–280 nm).

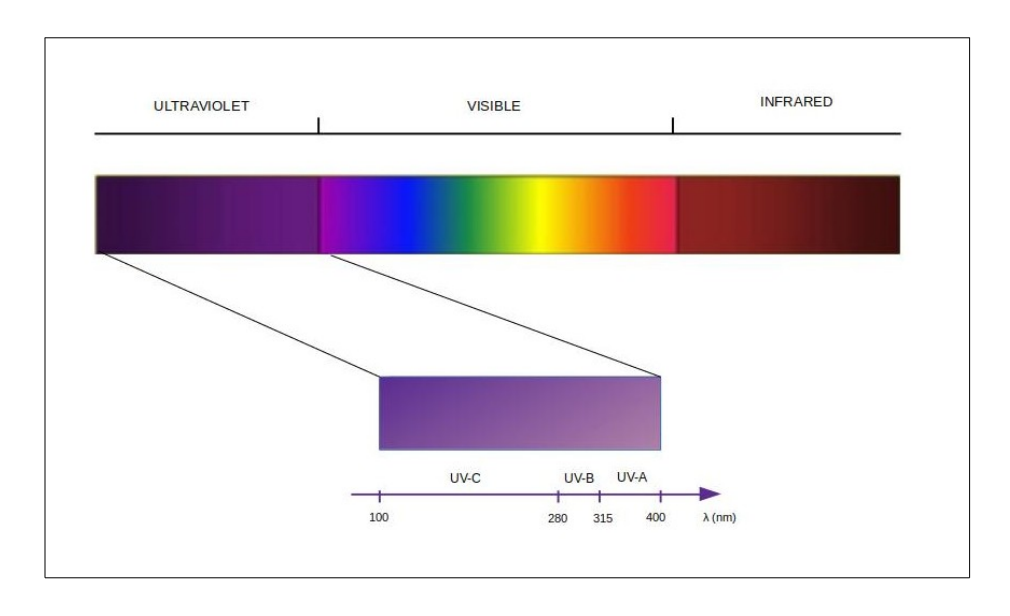


Figure 1.7 – Ultraviolet radiation spectrum

The atomic, molecular and ionic composition of the upper atmosphere depends rather critically on the character on solar emissions and their interactions with the atmospheric gases. Although occurring high in the atmosphere, these interactions are important to life on the earth's surface. As sunlight passes through the atmosphere, all UVC and approximately 90% of UVB radiation are absorbed by ozone, water vapour, oxygen and carbon dioxide. UVA radiation is less affected by the atmosphere. Therefore, the UV radiation reaching the Earth's surface is largely composed of UVA with a small UVB component. UV radiation is able to interact with organic molecules harming biological organisms generating phenomena as tan, freckles, sunburn and in extreme situations skin cancers and cataracts in humans. Moreover an increase in UV radiation generates a decrease of photosynthetic productivity in terrestrial and marine ecosystems as well as agricultural crop yield. UV radiation levels arriving at a location on Earth are influenced by Sun elevation (UV levels are higher especially at midday in the summer), latitude (UV levels are higher at equator than poles), cloud cover (UV levels decrease with increase of cloud coverage), altitude (every 1000 m of height UV levels increase by 10-12%), ground reflection (albedo) and atmospheric ozone content. In general, ozone absorbs 1,5% to 3% of the solar radiation incident on the atmosphere, depending on solar elevation and total ozone content. Even if ozone is a minor constituent of the earth's atmosphere it plays a major role as an atmospheric absorber of radiation in the UV wavelength range 200 - 350 nm.

In the 1970s, it was recognized that the ozone layer was threatened by the use of ozone-depleting substances (ODSs), chemicals such as chlorine-containing chlorofluorocarbons (used for refrigeration, air conditioning, and other applications), bromine-containing Halons (used for fire suppression), and many other chemicals containing chlorine and bromine. These human-emitted chemicals have their most dramatic impact in the annual Antarctic ozone hole, a phenomenon that started in the late 1970s and recognized in the early 1980s. To limit the adverse effect of human activity on ozone, in 1985 there was The Vienna Convention for the Protection of the Ozone Layer and in 1987 The Montreal Protocol on Substances that Deplete the Ozone Layer (the Montreal Protocol) was signed. The Montreal Protocol is an international agreement designed to stop the production and import of ozone depleting substances and reduce their concentration in the atmosphere to help protect the earth's ozone layer. The treaty entered into force in 1989 and over the years has been subjected to revisions in 1990 (London), 1992 (Copenhagen), 1995 (Vienna), 1997 (Montréal) and 1999 (Beijing). The European Union (EU) and its member countries take part in international efforts to fight climate change under the UN climate convention. The United Nations Framework Convention on Climate Change (UNFCCC), agreed in 1992, is the main international treaty on fighting climate change. Its objective is to prevent dangerous man-made interference with the global climate system. The UNFCCC's top decision-making body is the annual_Conference of the Parties (COP). All Parties to the Convention can take part. Representatives of business, international organizations, interest groups and associations have observer status.

Ozone is measured throughout the atmosphere with instruments on the ground, on board aircraft, high-altitude balloons, and satellites. Some instruments measure ozone directly in sampled air and others measure ozone remotely some distance away from the instrument (Figure 1.8). Instruments use optical techniques with the Sun (passive instruments as spectrophotometers - e.g. BREWER, or active instruments that use and lasers as light sources, e.g. LIDAR) or use chemical reactions that are unique to ozone (e.g. ozone sounding). At many locations over the globe, regular measurements are made to monitor total ozone amounts and their variations over time.

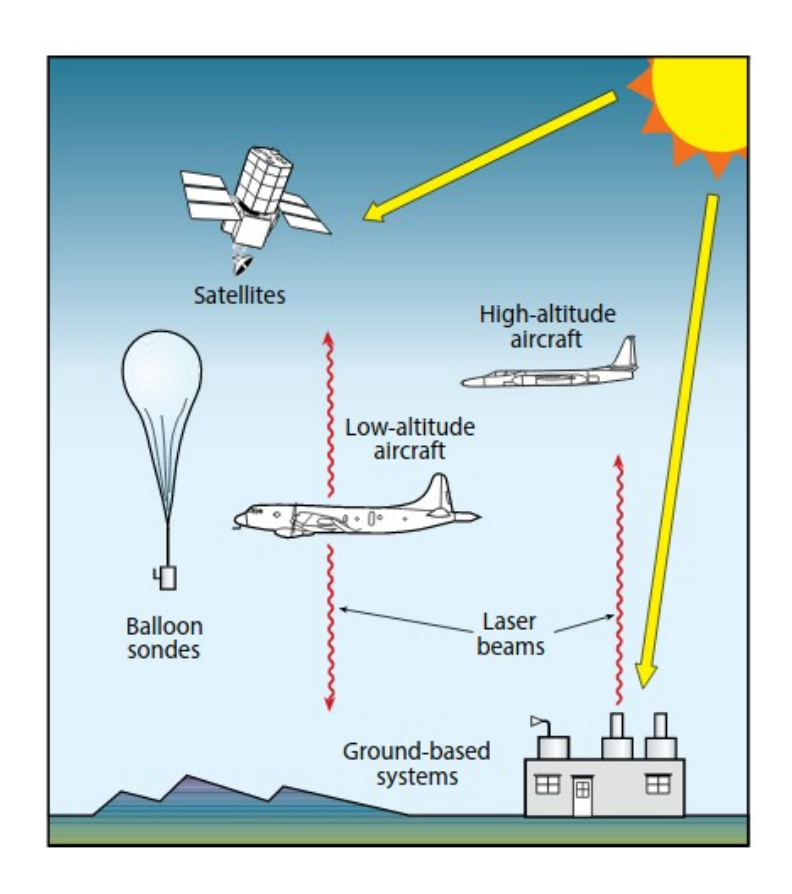


Figure 1.8 – Ozone measurements. - (Courtesy of R.J. Salawitch and coauthors, 2018)

Chapter 2

THE MEASUREMENT OF TOTAL OZONE ABOARD SATELLITE

2.1 – Objectives

This chapter describes how the Total Ozone Mapping Spectrometer (TOMS) and the Ozone Monitoring Instrument (OMI) operate aboard satellite. Relevant algorithm and techniques are illustrated showing how, starting from backscattered radiance measurements in the UV region, is possible to infer the total ozone column value.

2.2 – The Total Ozone Mapping Spectrometer TOMS

In the past, measurements of total ozone column amount were conducted since 1978 with the instruments aboard both the NASA Nimbus-7 satellite and the Russian Meteor-3 satellite until the instrumentation end of operational life in December 1994. In July 1996, the Total Ozone Mapping Spectrometer (TOMS) was launched aboard the Earth Probe (EP), a sun-synchronous LEO satellite at an altitude of 780 km, to provide NASA with long-term values of the total column ozone distribution over the whole globe. The TOMS carries out 35 measurements every 8 seconds, covering an area on the earth's surface with a width between 50 and 200 Km (Instant Area Access). Every day the earth's surface is completely covered excepted the areas near one of the poles where the Sun is low or below the horizon. The TOMS is a second generation instrument that performs an indirect measurement of ozone starting from a direct measurement of solar radiation and its backscattered fraction from the Earth's atmosphere towards the satellite in the near ultraviolet region of the electromagnetic spectrum. In this region of the spectrum, UV radiation is only partially absorbed by the atmosphere itself. The latest version (V.8) of the algorithm for processing TOMS data is described below. From an operational point of view, the calculation of total ozone is based on the comparison between the measurement of normalized radiance and the radiance derived using a radiative transfer model called TOMRAD.

The final ozone value is obtained through a series of steps:

1) Measurement of radiance

The TOMS measures both the UV radiation emitted by the Sun and the backscattered UV radiation from the Earth's atmosphere at six wavelengths (308,6-313,5-317,5-322,3-331,2-364,4 nm). A portion of the radiation emitted by the Sun reaches the layers of the lower Earth's atmosphere, undergoes the scattering process by air molecules and by the upper part of the clouds and is backscattered towards the sensor located on the satellite. Along the way to the earth's surface, a fraction of the UV radiation emitted by the Sun, passing through the stratosphere, is absorbed by ozone.

If the function linking the normalized radiance to the amount of ozone is known:

$$I = f(O_3)$$
 (2.1)

then using an inversion technique it is possible to obtain the ozone value from the radiance measurement.

$$O_3 = f^{-1}(I)$$
 (2.2)

where:

I= normalized radiance;

 O_3 = ozone value.

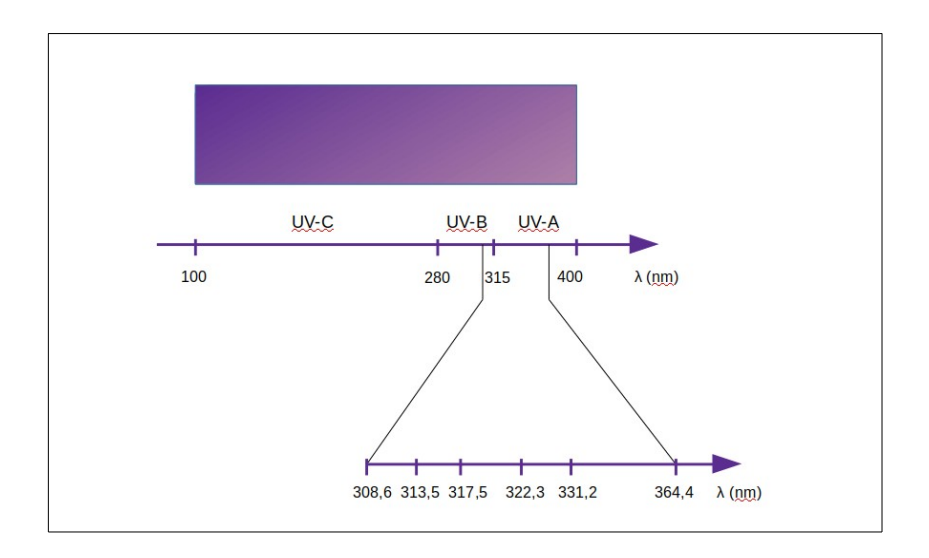


Figure 2.1 - Wavelengths used by TOMS

2) The radiative transfer model TOMRAD

In order to determine the relationship between the radiance and the ozone value, a radiative transfer model is used.

The radiance is calculated using the following equation:

$$I = I_0(\theta_0, \theta) + I_1(\theta_0, \theta) \cos\varphi + I_2(\theta_0, \theta) \cos 2\varphi + \frac{RI_R(\theta_0, \theta)}{1 - RS_b}$$
(2.3)

where

 θ_0 = solar zenith angle

 θ = satellite zenith angle

 ϕ = azimuth angle between the plane containing the Sun and the local nadir and the plane containing the satellite and the local nadir

R = reflectivity

 I_R = radiance due to reflection

 S_b = term that is introduced to take into account multiple reflections in the atmosphere and that dimensionally it is equal to the inverse of reflectivity.

The first three components in (2.3) represent the contribution due to the atmosphere (I_a)

$$I_{a} = I_{0}(\theta_{0}, \theta) + I_{1}(\theta_{0}, \theta)\cos\varphi + I_{2}(\theta_{0}, \theta)\cos2\varphi \tag{2.4}$$

while the last term represents the contribution due to reflection.

The model considers surfaces as Lambertians, ideal surfaces reflecting incident energy from one direction in the same way in all directions.

From an operational point of view, on output are generated tables, that are calculated for 10 solar zenith angles, 6 satellite zenith angles and 4 pressure surfaces, selected in such a way that radiance errors respect to the values derived from climatology are lower than 0.1%.

Moreover, since the model has been developed considering an elastic scattering, corrections are applied to take into account the non elastic rotational Raman scattering. Light of a given frequency interact with a molecule possessing a permanent dipole moment to leave it in a different rotation state than the one in which it was originally found.

To establish the relationship that links the radiance to the vertical ozone profile and to the vertical temperature profile, 21 standard ozone profiles, varying with the total ozone content and with the latitude, were used. The profiles were generated using ozone soundings data below 25 km and using data collected by NASA's SAGE II instruments (Stratospheric Aerosol and Gas Experiment), launched in October 1984 aboard the Earth Radiation Budget Satellite (ERBS) for higher altitudes.

The atmosphere is sliced into 10 layers of about 4.8 km thick, extending from the pressure of 1 atm (1013 hPa) up to 2⁻¹⁰ atm and initially, using an average profile for the temperature, the radiance in each layer is determined for each of the standard ozone profiles by means of interpolations. Then corrections are applied varying the temperature profile. A data set corresponding to 1512 profiles is generated on output. In case of clouds, the pixel seen from the satellite is partially opaque. In addition, the correction due to the presence of clouds, which are assimilated to an opaque Lambertian surface, is applied to the radiance values using the following equation:

$$I = I_s(R_s, p_s)(1 - f_c) + I_c(R_c, p_c)f_c(5)$$
 (2.5)

where

 I_s = radiance of the portion of the pixel not covered by clouds

p_s = pressure at a certain model altitude

 R_s = reflectivity of the Lambertian surface corresponding to a pressure level p_s

 f_c = clouds portion

 I_c = radiance of the portion of the pixel covered by clouds

 p_c = pressure at a certain altitude

 R_c = reflectivity of the Lambertian surface corresponding to the pressure level p_c

Within the model, an average value R_c =0.8 is assumed.

3) Ozone evaluation from the radiance measurement

The basic version of the TOMS V8 algorithm uses only two of the six wavelengths for the evaluation of total ozone indicated in figure 2.1. The wavelength 331.2 nm, at which UV radiation from the Sun is insensitive to the ozone absorption, is used for the estimate of reflectivity (or the effective fraction of clouds). The wavelength 317.5 nm, at which UV radiation is highly absorbed by ozone, is used for the estimation of the atmospheric constituent. As in the typical case of remote sensing algorithms based on inversion, it is necessary to use a first guess to obtain the solution. In the case considered the first guess is represented by the data set consisting of 1512 profiles of TOMRAD. For a given latitude and for a given month this dataset provides from 3 to 10 profiles that vary with total ozone and that allow to establish a unique mathematical relationship between the radiance derived from the TOMS at 317.5 nm and the total ozone.

Initially, an estimate of the effective reflectivity respect to fraction of the clouds is made using the inverse equation:

$$R = \frac{(I_m - I_a)}{I_R + S_b(I_m - I_a)} \tag{2.6}$$

where

R = reflectivity

 I_m = radiance measured at the wavelength 331.2 nm

 I_a = radiance due to the atmosphere

 I_R = radiance generated by reflection

 f_c = clouds portion

If R < 0.15 the algorithm assumes that there are no cloud, while in all the other cases the cloud fraction is estimated assuming $R_s = 0.15$ and $R_c = 0.8$. in the equation:

$$I = I_s(R_s, p_s)(1 - f_c) + I_c(R_c, p_c)f_c$$
 (2.7)

obtaining from (2.7)

$$f_c = (I_m - I_s)/(I_c - I_s)$$
 (2.8)

If $f_c > 1$, the contribution of the surface to the radiance is assumed zero and the actual reflectivity of the cloud is calculated using the following relationship assuming that the surface is at p_c .

$$R = \frac{(I_m - I_a)}{I_R + S_b(I_m - I_a)} \tag{2.9}$$

Using R value from (2.9) or f_c value from (2.8), it is possible to define a relationship between the radiance at 317.5 nm and the total ozone using the a priori profiles.

Starting from the 21 standard profiles, we can estimate the total ozone Ω_0 .

Then using this Ω_0 value, a single a priori x_{ap} profile, from which the radiance corrections are calculated, is selected within the data set of the 1512 profiles, taking into account the effect of the atmospheric temperature. In many cases these corrections are less than 2%, but they can also reach values of 10% for high zenith angles (85°)

These corrections lead to a new total ozone a priori value Ω_{ap} :

$$\Omega_{ap} = \Omega_0 - (\ln I_{ap} - \ln I_0) / \frac{\partial \ln I_{317,5}}{\partial \ln \Omega}$$
 (2.10)

The Ω_{ap} value represents the best estimation of the total ozone Ω_{best} , which is therefore dependent not only on the a priori profile but also on the change in the logarithm of the radiance measured at 317.5 with the total ozone.

In reality the relationship that links the logarithm of the radiance to the ozone is slightly non-linear, with the consequence that the total ozone corresponding to the radiance measurement is estimated by means of a piecewise linear interpolation and the quantity $\partial \ln \Omega$ represent the slope of the piecewise curve. Figure 2.2 shows a theoretical image of the

interpolation process showing that the more the extrapolated curve approaches the real one, the more the estimated ozone data will approach the real one. The matching between the two curves will depend on the values of the variation of the radiance logarithm with ozone at the different levels.

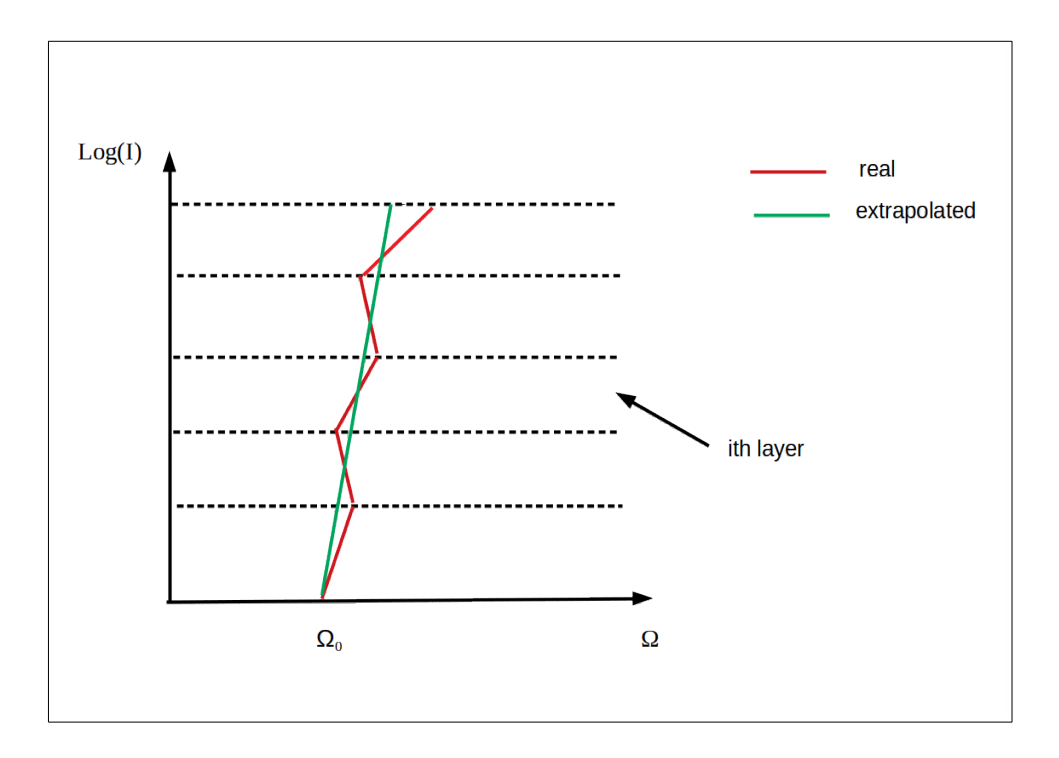


Figure 2.2 – Theoretical image of the interpolation process

The deviation of the inferred total ozone value Ω_{best} from the true value Ω can be obtained as follows:

if we indicate with χ the ozone content relative to an atmospheric layer, the efficiency factor of the layer is defined as:

$$\eta_i = \frac{\partial \ln I}{\partial \ln \chi_i} / \frac{\partial \ln I}{\partial \ln \Omega}$$
 $i = 0, \dots, 9$ (2.11)

which provides information on how much in each atmospheric layer the estimated ozone value really represents the real ozone value.

From (2.12) it is possible to write the relationship between the true total ozone Ω and the calculated total ozone Ω_{best} as:

$$\Omega_{best} = \Omega - \sum_{i=0}^{9} (1 - \eta_i) (\chi - \chi_{ap})_i$$
 (2.12)

where

 χ_{ap} = a priori ozone value in a given layer χ = true ozone value in a given layer

From (2.12) we have that the more the estimated ozone value will be close to the real one the more χ_{ap} will approach χ and the more the efficiency factor of the layer η_i will be equal to 1.

In reality, what happens is that with the exception of high zenith solar angles, the values of η_i are close to 1 in all layers except for layer 0, which is relative to the lower troposphere and is strongly characterized by Rayleigh scattering and the presence of clouds.

In some cases, due to the presence of snow or low clouds, values of η_0 even greater than 1 can occur. For high zenith solar angles in the average stratosphere η_i assumes values greater than 1 with the consequence that there will be an underestimation of ozone in the upper layers.

Corrections to the estimated total ozone values can be made if additional data relating to aerosols, to the effects due to sea reflections (Sea-glint) and to other atmospheric components, such for example sulfur dioxide (SO_2), are available. Corrections to the a priori ozone profile can be made using the measurements made by the TOMS at the other wavelengths.

2.3 - The Ozone Monitoring Instrument (OMI)

On July 15th 2004, the Ozone Monitoring Instrument (OMI) onboard the National Aeronautics and Space Administration's (NASA) Earth Observing System (EOS) Aura satellite was launched. Aura, from the Latin word breeze, was launched into a sun-synchronous, near polar (98.2 degree inclination) orbit. It orbits 705 km above the Earth with a sixteen-day repeat cycle and 233 revolutions per cycle. The ascending node is in daylight and crosses the equator at approximately 1:45 PM. The Aura spacecraft is flying in formation with other Earth observing satellites called the A-Train. Aura's instruments measure trace gases in the atmosphere by detecting their unique spectral signatures. Data taken by the satellite instruments are stored on board until broadcast to a downlink facility through the spacecraft's high speed data link. Because polar orbiting satellites frequently pass over the Arctic and Antarctic, the data downlink facilities are located at high latitudes. NASA's major downlink facilities are Poker Flat, Alaska, McMurdo Base, Antarctica and Svalbard, a Norwegian archipelago in the Arctic Ocean north of mainland Europe. Once the data are received at the downlink facility, they are sent via optical fibre network to processing facilities at NASA's Goddard Space Flight Center. The raw data are then distributed to the instrument teams for processing into geophysical measurements. Processed data are sent to NASA Data Active Archive Centers, where they are made available to users. The Aura satellite also has direct broadcast capability through a smaller downlink antenna. This capability allows an investigator to receive data in near real time. Finnish direct broadcast station receives OMI data as the satellite passes overhead. The direct broadcast data are processed at the Finnish Meteorological Institute (FMI) and distributed shortly after the Aura overpass.

The OMI is the first of a new generation of spaceborne spectrometers that combine a high spatial resolution ($13 \times 24 \text{ km}^2$ at nadir) with daily global coverage. OMI derives its heritage from NASA's Total Ozone Mapping Spectrometer (TOMS) instrument and the European Space Agency (ESA) Global Ozone Monitering Experiment (GOME) instrument (on the ERS-2 satellite). It can measure many more atmospheric constituents than TOMS and provides much better ground resolution than GOME ($13 \times 25 \text{ km}^2$ for OMI vs. $40 \times 320 \text{ km}^2$ for GOME). The instrument is a contribution of the

Netherlands's Agency for Aerospace Programs (NIVR) in collaboration with the Finnish Meteorological Institute (FMI) to the Aura mission.

OMI allows to derive the total columnar ozone value using the Differential Optical Absorbption Spectroscopy (DOAS).

The OMI total ozone DOAS algorithm consists of three steps:

1) Slant column density derivation

The DOAS method is used to fit the differential absorption cross section of ozone to the measured sun-normalized Earth radiance spectrum. This fit is computed in a well defined range of wavelengths called the *fit window*.

The aim is to obtain the slant column density, which is defined as the amount of ozone along the average path crossed by photons from the Sun, which are backscattered from the atmosphere towards the sensor aboard the satellite. The photons reach the instrument through many paths that contribute to the slant column density that will depend on the scattering and absorption processes in the atmosphere and the reflection of the surface (Figure 2.3).

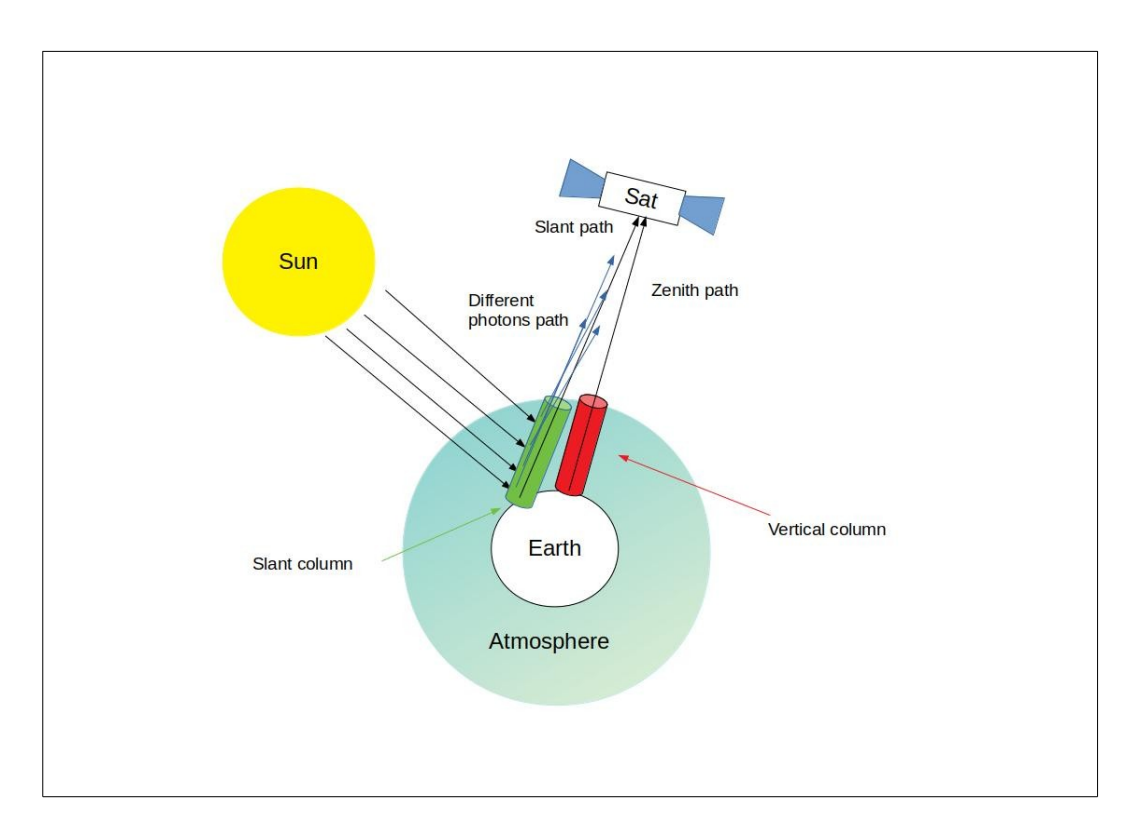


Figure 2.3 - Ozone slant and vertical colums.

From an operational point of view, is defined a polynomial function (fit function) which operates as a high pass filter and which is applied to take into account the absorption and scattering processes that vary gradually with the wavelength, the surface reflection, the properties of atmospheric constituents and clouds. The mathematically defined high pass filter needs adjustments that correspond in some way to a radiometric calibration.

The instrument measures the backscattered radiation from the earth's surface and atmosphere in the wavelength range between 270-500 nm. Notwithstanding ozone absorbs in the full considered wavelength range (figure 2.4), to determine the ozone amount only wavelengths below 340 nm are used, because the cross section values show that the absorption is enough significant to provide realistic measurements only at these wavelengths.

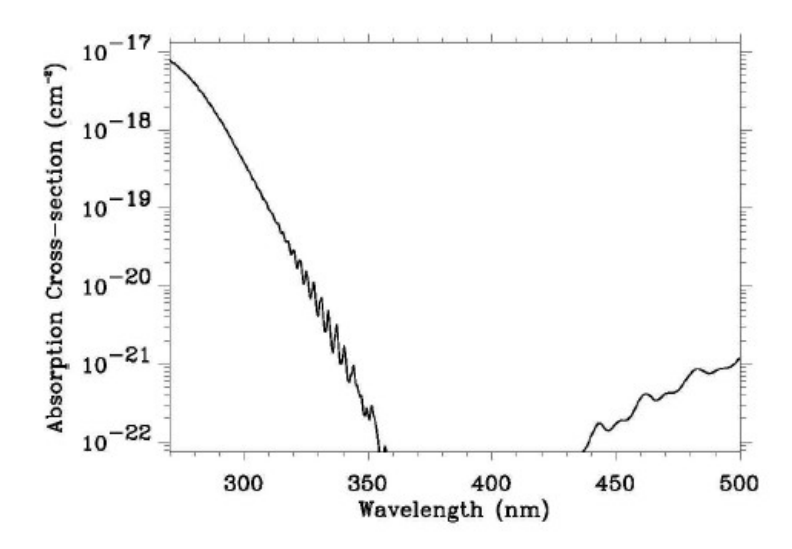


Figure 2.4 - O_3 Absorption Spectrum in the wavelength range 270 - 500 nm (Courtesy of P.K. Bhartia - 2002)

The *fit function* used in the OMI alghorithm is:

$$\frac{I(\lambda)}{F(\lambda)} = P(\lambda) \exp[-N_s \sigma_{O3}(\lambda, T_{eff})]$$
 (2.13)

where

 λ = wavelength

I = radiance

F = extraterrestrial solar irradiance

P = polynomial

 N_S = Slant column density

 σ_{O3} = ozone absorption cross-section

 T_{eff} = effective ozone temperature

The ozone absorption cross-section depends on the effective temperature, and this is treated within the DOAS by linearizing the cross-section around T_0 :

$$\sigma_{O3}(\lambda, T_{eff}) = \sigma_{O3}(\lambda, T_0) + (T_{eff} - T_0) \frac{d\sigma_{O3}}{dT}(T_0)$$
 (2.14)

Equation (2.14) expresses the fit function above mentioned, and it is accurate only in the case of elastic scattering. In reality, about 6% of light scattering events inside the fit window are inelastic, which means that the light leaving the scattering process has a different wavelength from the incoming light. As a consequence, the value of the slant column density is underestimated with values between 3% and 10%. The main effect of inelastic scattering is due to the Raman rotational scattering, well described by the phenomenon known in literature as the Ring effect. To consider this effect, the *fit function* is modified as follows:

$$\frac{I(\lambda)}{F(\lambda)} = P(\lambda) \exp\left[-N_s \sigma_{O3}(\lambda, T_{eff})\right] + c_{ring} \frac{I_{ring}(\lambda)}{F(\lambda)} \exp\left[-N_s \sigma_{O3}(\lambda, T_{eff})\right]$$
(2.15)

where

 $I_{\mbox{\tiny ring}}$ = the convolution of extraterrestri al solar irradiance with the Raman spectrum

 c_{ring} = fit parameter to scale the radiance due to Raman scattering, which depends on the thickness of the Ring lines in the *fit window*

 σ_{03} = ozone absorption cross-section partially modified by the Raman scattering

The fit parameters (N_s , T_{eff} , c_{ring} , polynomial coefficients) are determined using a non-linear, least squares fit. Information on the quality of the fit and the fit parameters is derived from the associated covariance matrix.

For the ozone cross sections are used reference values obtained on an experimental basis from ground measurements and ozone soundings. The values are adapted by a convolution to the spectral response of the OMI (*slit function*).

In figure 2.5 the Radiance Contribution Functions (RCF) at different wavelengths in function of height, for a 45° zenith angle are showed. The curves represent the contribution of the backscattered radiation that is received by the instrument located on the satellite.

It can be note that around 305 nm the RCF is extremely large at different levels, while at longer wavelengths there is a peak in the troposphere and at shorter wavelengths there is a peak in the stratosphere.

Since 95% of the ozone is located at a higher altitude than the tropospheric peak, the radiation coming from the troposphere during its way to the instrument crosses almost the entire ozone layer in the atmosphere and therefore the measurements made at longer wavelengths of 310 nm are particularly suitable to derive total columnar ozone amount, while the measurements made around 300 nm are particularly suitable to obtain the ozone value in the lower stratosphere.

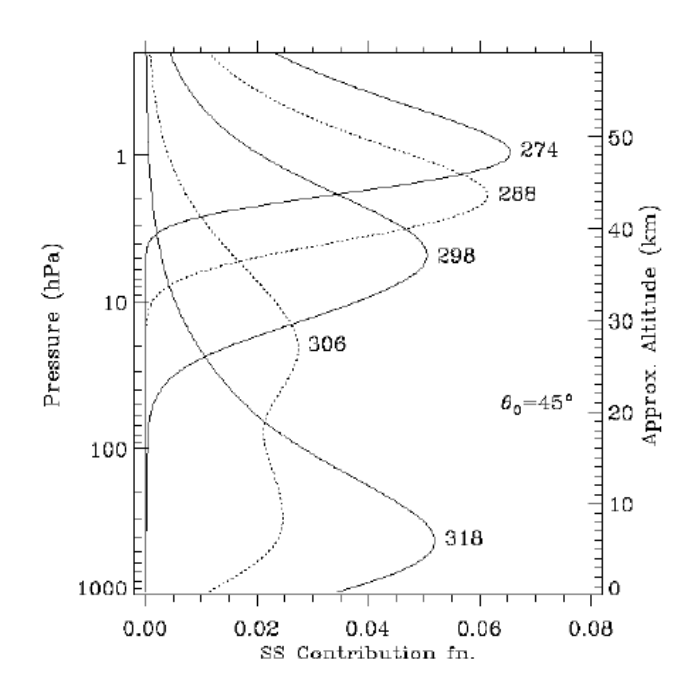


Figure 2.5 - Radiance Contribution Functions (RCF) at different wavelengths in function of height. - (Courtesy of P.K. Bhartia - 2002)

Detailed studies were conducted in order to identify the optimal *fit window* for OMI. The studies led to identify the main factors determining the dependence of the slant column density on the atmospheric temperature and in the signal / noise ratio, which places a lower limit on the width of the fit window. On the basis of these considerations, a window with a width of 5 nm centred around 334.1 nm was selected for the OMI. With this choice, a second degree polynomial is used in the high pass filter. The extension of the fit window towards shorter wavelengths, if on the one hand it would lead to a reduction of instrumental noise, on the other hand, would lead to an increase in the dependence on the temperature profile with the consequent reduction of the total accuracy of the fit due to the fact that DOAS would become less accurate for stronger absorptions (the cross section increases), the dependence on the ozone profile would increase and it would be necessary to introduce a higher order polynomial. The studies have shown that in addition to the window identified there are other windows that allow to obtain good performances, but the one identified is the best for the OMI.

2. Correction of the air mass factor

In the second step the slant column density is translated into the vertical column density. This is necessary because the path along which the light reaches the sensor on board the satellite is not directed along the vertical.

The ratio between the slant column density (N_s) and the vertical column density (N_v) is defined as air mass factor:

$$M = N_s / N_v$$
 (2.16)

The air mass factor will depend on the angle of view and the solar geometry, the fit window used, the surface albedo, the surface pressure, the vertical ozone profile, the clouds and the aerosols, because all these factors affect the density of the slant column.

The air mass factor is calculated by means of simulations of the measured spectrum to which the DOAS is applied. The simulations of the OMI spectrum are obtained using a radiative transfer model in combination with an OMI simulator. The simulator is used to transform the high resolution spectra obtained from the radiative transfer model into spectra that have the same resolution and are sampled as those characteristic of the OMI.

The fit function is applied to the simulated spectra in order to calculate the slant column density. Considering that for the simulated spectra the vertical column density is known in advance, the air mass factor can be calculated. The more the atmospheric model used for the calculation of the radiative transfer reproduces the real atmosphere, the more the value of the calculated air mass factor is accurate. The air mass factor is pre-calculated and stored in the lookup table as a function of the Sun-satellite geometry, ground pressure, latitude, month and ozone content. The ground pressure is derived from the altitude of to the pixel representing the ground relative to the standard pressure at the sea level equal to 1013 hPa. The ozone profiles used are based on the climatology of the TOMS observation data. The surface albedo is derived from the combination of data obtained from the TOMS climatology with data relating to the snow cover and the percentage of water / ice coverage present.

3. Clouds correction

The third step is to apply the correction due to the presence of clouds.

When a pixel of the ground is partially or completely covered by clouds, the algorithm must take into account both the effect that is produced on the air mass factor and the obscuring of a portion of the ozone column which occurs in an instrument placed on the satellite.

To calculate the correction to apply to the air mass factor, a cloud cover model is used representing clouds on Lambertian surfaces, ideal surfaces that reflect incident energy from one direction homogeneously in all directions, located at an altitude corresponding to the cloud pressure.

For these surfaces, an albedo equal to 0.8 is assumed, such a value providing the best results for calculating ozone with the DOAS technique. The model considers as if all the clouds are thick as a single layer. For pixels with partial coverage, the correction is applied as a percentage.

Using this model, the air mass factor for the pixels affected by cloud cover is calculated in the same way is done for the pixels without coverage using the following relationship:

$$M = w \cdot M_{cloudy} + (1-w) \cdot M_{clear}$$
 (2.17)

where the weight w is the fraction of the radiance which is due to the portion of the pixel covered by the clouds.

The ozone amount below the Lambertian cloud is defined as "ghost column" (N_g) and it is calculated by considering the ozone profile between the ground and the height of the cloud by measuring the corresponding slant column density.

Then the vertical columnar content N_{ν} is calculated using the following equation:

$$N_{v} = \frac{N_{s} + w \cdot M_{cloudy} \cdot N_{g}}{M}$$
 (2.18)

Chapter 3

THE MEASUREMENT OF TOTAL OZONE AT GROUND

3.1 – Objectives

This chapter describes how the BREWER spectrophotometer operates at ground. A description of the instrument is showed. The processing algorithm is illustrated showing how, starting from direct radiance measurements in the UV region, is possible to infer the total ozone column value.

3.2 - The BREWER Spectrophotometer

The BREWER Spectrophotometer is a scientific instrument, which measure ultraviolet radiation (UV) in the solar spectrum. The BREWER was originally designed for the measurement of Ozone as part of the World Meteorological Organization (WMO) - Global Atmosphere Watch (GAW) programme.

At present time BREWER (MKIII version) produced by Kipp & Zonen, is the only instrument sanctioned by the WMO for making total column ozone measurements. By examining the differential absorption of select wavelengths in the UVB portion of the spectrum, determinations of total column ozone is inferred. In addition, accurate spectral intensity profiles of UV radiation in the 286.5 nm to 363 nm range are measured.

The complete BREWER system is comprised of the following:

- Spectrophotometer
- Solar Tracking System
- Personal Computer operating Software

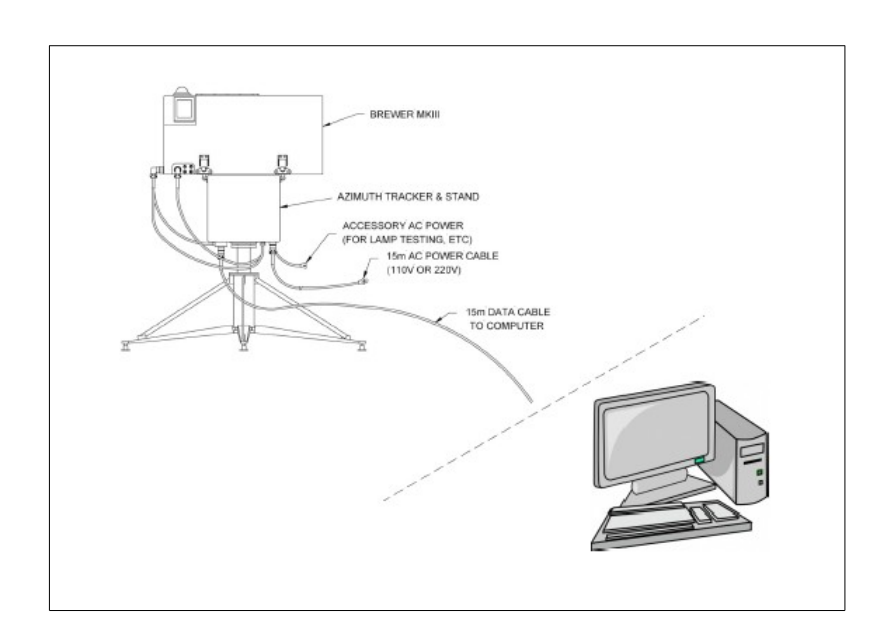


Figure 3.1 – The BREWER system - (Courtesy of Kipp & Zonen)

The instrument can operate in manual, semi-automated or in fully-automated mode. In both manual and semi-automated modes the operator start a specific observation or instrumental test by typing a simple 'command' on the computer keyboard. In the fully-automated mode, a schedule in the computer controls all operations. Raw data are automatically recorded on the computer data drive, and ozone and UV results are available in real time.

3.3 - Spectrophotometer

The spectrophotometer, is an optical instrument designed to measure ground-level intensities of the attenuated solar UV radiation. The BREWER is designed for continuous outdoor operation and is therefore housed in a rigid weatherproof shell protecting the finely tuned internal components. The instrument reliably and accurately operates over a wide range of ambient temperature and humidity conditions. The weatherproof case is built on two parts: a base, which all optical and electronic assemblies are anchored on and a removable cover. In figure 3.2 a detail of the external top view of the instrument is showed. The BREWER instrument control panel can be viewed through a perspex window in the top of the cover. Viewing ports for both the iris and the spectrometer entrance slit are visible through this window. In one corner of the cover is a 14 cm deep, 35° inclined surface. A 6.35 cm by 14 cm hole has been cut from this surface to provide an opening which is properly positioned to pass direct sunlight or zenith skylight to the spectrophotometer. This opening is covered by a quartz window, which is secured by a weatherproof seal. Three circular weatherproof connectors for power supply, communication signals, motor control and monitor signals for the azimuth tracker are mounted on the side of the BREWER base below the weatherproof seal.

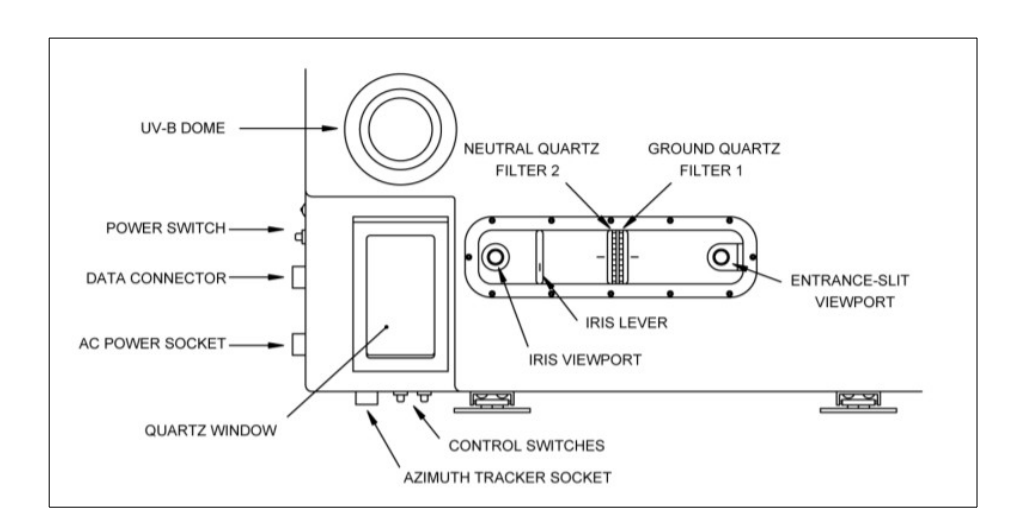


Figure 3.2 – External top view detail of the spectrophotometer. (Courtesy of Kipp & Zonen)

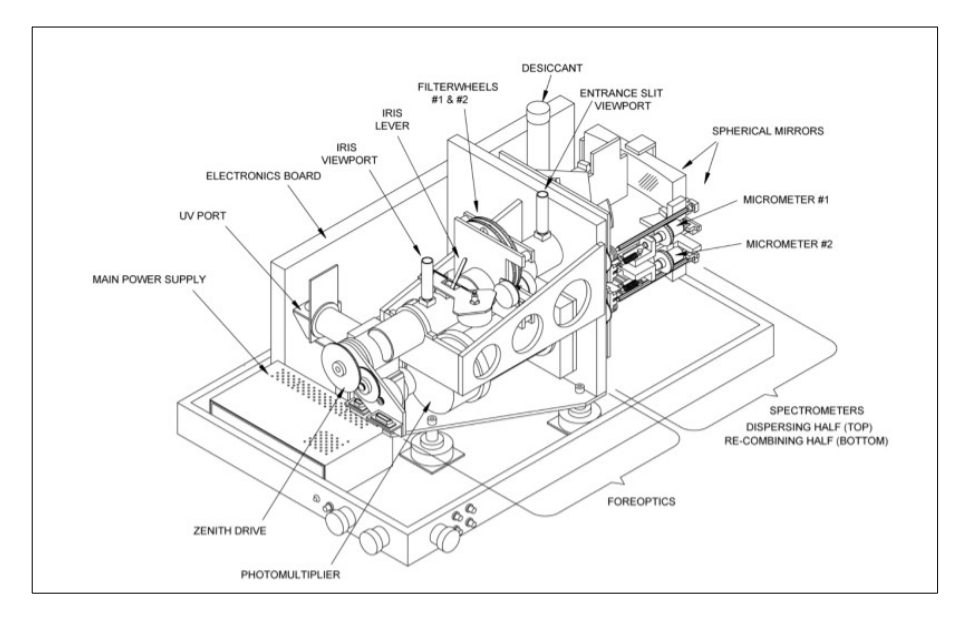


Figure 3.3 – View of the instrument with cover removed. (Courtesy of Kipp & Zonen)

In figure 3.3 a view of the instrument with cover removed is showed. The spectrophotometer is comprised of the following:

Foreopticts

Across a quartz window, the incoming radiation reach a right-angle zenith prism to be directed to the spectrometer by means of a lens system. The right-angle zenith prism allow to direct to the optical axis of the instrument the incoming light from the sun, the sky, or the test lamps. For zenith angles in the range 0° to 90° the sun, or sky, is viewed through an inclined quartz window. At zenith angle 180° the spectrometer views the calibration lamps; at -90° the UV diffuser occupies the field-of-view (Figure 3.4). The prism is mounted in a retainer which rotates in a dual-bearing system. The prism is rotated by a microprocessor controlled zenith stepper motor through a 270-degree rotation range.

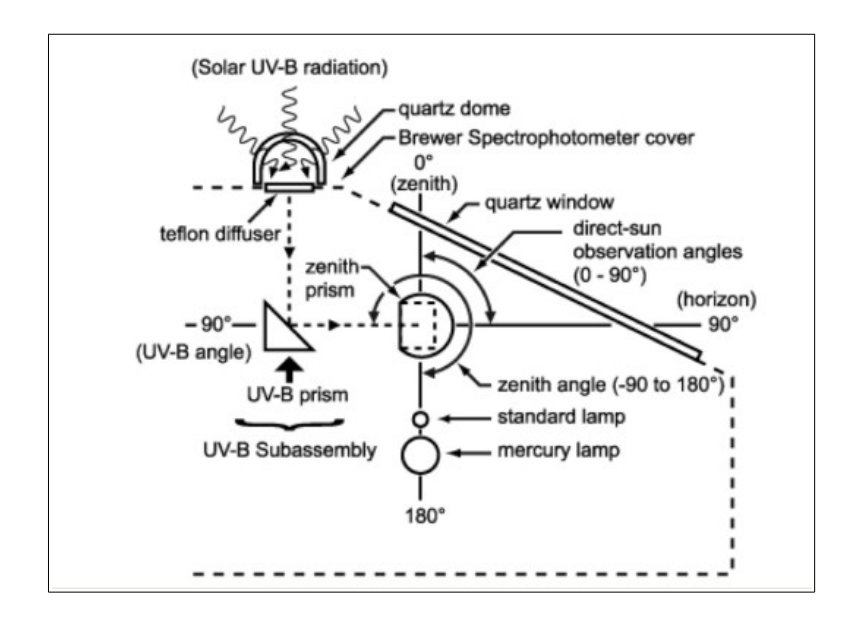


Figure 3.4 – Zenith prism view. - (Courtesy of Kipp & Zonen)

A quartz-halogen lamp is located under the zenith prism. The lamp provides a wellregulated light source which is used as a reference for sensitivity measurements. Beneath the halogen lamp is a mercury discharge lamp, which provides a line source for wavelength calibration. Ultraviolet radiation from the mercury lamp passes through the halogen lamp to the zenith prism. In figure 3.5 a top view of BREWER is showed. Incoming light is directed through the foreoptics by the director prism. Elements in the foreoptics provide adjustment for field-of-view, neutral-density attenuation, ground-quartz diffusion, and selection of film polarizers. An iris diaphragm is mounted in the foreoptics at the ultraviolet focus of a planoconvex lens. The iris select the light amount entering in the spectrometer. The lens focuses ultraviolet objects at infinite distance onto the plane of the iris. When the instrument is aligned to view sunlight, an image of the sun is focused at the centre of the iris. On the spectrometer side of the iris there is another plano-convex lens positioned such that its focal point is in the plane of the iris. After the iris there are two filterwheels mounted in a filterwheel housing. Each wheel has six 25.4 mm diameter holes spaced at 60 degree intervals. Each hole can be selected to intersect the optical axis by rotating its filterwheel. The first filterwheel includes polarization filters used for different type of measurements (total ozone, UV, ozone profile, etc.). The second filterwheel contains an open hole and five neutraldensity filters providing different attenuation used to automatically adjust the intensity of the light entering the spectrometer. An 11.18 mm fixed aperture located on the spectrometer side of the filterwheel housing limits the field-of-view of the spectrometer to f/6.

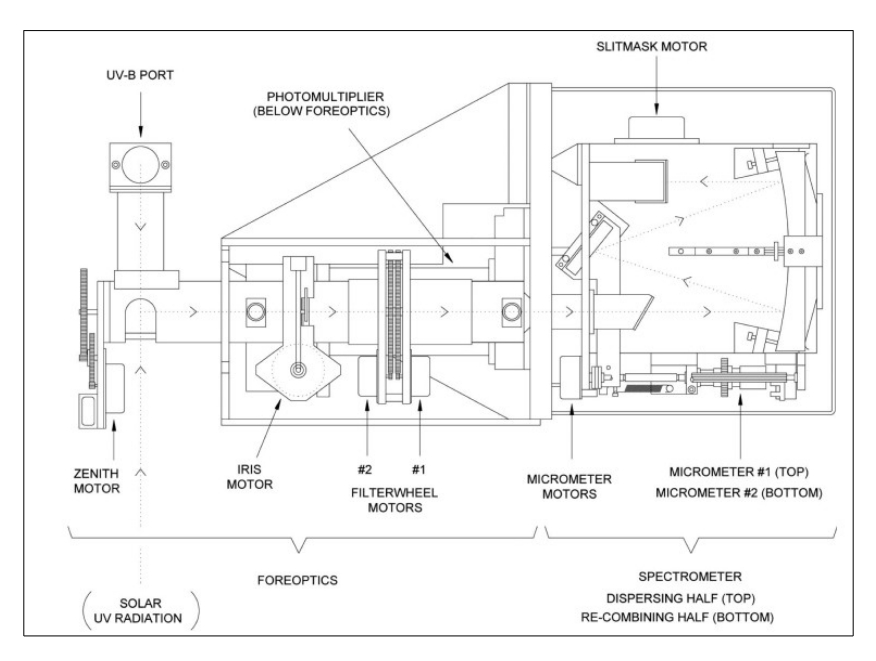


Figure 3.5 - Top view of BREWER - (Courtesy of Kipp & Zonen)

Spectrometer

The BREWER contains two modified Ebert spectrometer, with focal length 16 cm and aperture ratio f/6, each utilizing 3600 line/mm holographic diffraction gratings operated in the first order. The gratings have optimum efficiency over the range 225 to 450 nm. The incoming radiation is acquired by the instrument and then is dispersed in a high quality spectrum on the focal plane of an exit slit. Six exit slits are positioned at the ozone operating wavelengths 303.2 nm (used for mercury-wavelength calibration), 306.3 nm, 310.1 nm, 313.5 nm, 316.8 nm and 320.0 nm with 0.6 nm resolution.

Light enters the entrance slit and in the first spectrometer is collimated by a spherical mirror onto a diffraction grating where it is dispersed. A second mirror reflection focuses the

spectrum onto the focal plane of a slotted cylindrical slit mask positioned at the entrance of the second spectrometer. Metric micrometer, rotated by stepper motors, are used to adjust the grating rotation. Following wavelength selection by the slit mask, the light passes through the second spectrometer where it is recombined and directed onto the exit slit plane. The six exit slits are located along the focal plane at the appropriate wavelength positions. Wavelength is adjusted by rotating the gratings with stepper motors which drive micrometers acting on lever arms. The wavelength-calibration procedure is capable of measuring the wavelength setting with a precision of 0.0001 nm, and of controlling the wavelength setting to 0.006 nm. The cylindrical mask exposes only one wavelength slit at a time. The mask is positioned by a stepper motor which cycles through all five operating wavelengths, approximately once per second. The cylindrical mask may be located in one of eight positions. The mask position 0 is used for mercury-wavelength calibration. The mask position 1 blocks light from all slits so that a dark count measurement can be made. The mask positions from 2 to 6 are used to infer ozone. The mask position 7 exposes two of the exit slits so that the dead time of the photon counting system may be determined. The correspondence between slit mask position and selected wavelength is summarized in Table 3.1.

Slit mask position	UV Wavelength Setting (nm)	
0	Hg Slit: 303.2 nm (Cal=302.1)	
1	Dark Count:	
2	Wavelength 1: 306.3	
3	Wavelength 2: 310.1	
4	Wavelength 3: 313.5	
5	Wavelength 4: 316.8	
6	Wavelength 5: 320.0	
7	Wavelength 2 & 4 for Deadtime Test	

Table 3.1 - Slit mask position vs nominal wavelength.

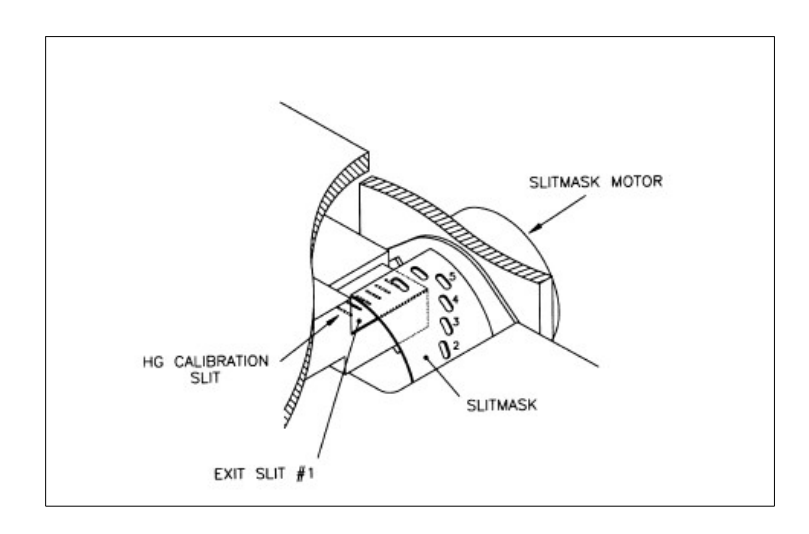


Figure 3.6 - Slit mask assembly (Courtesy of Kipp & Zonen).

• Photomultiplier Detector (PMT)

Light passing through the exit slits is collected by means of a low-noise PMT detector. Radiation through the exit slits is focused onto the cathode of the PMT located at the ultraviolet focus of the Fabry lens. The photon pulses are accumulated and amplified, scaled by means of a pulse amplifier. Then the photon pulses are transmitted to a counter and the resulting photon count is registered in one of six wavelength channels. The PMT is enclosed in a magnetic shield which is maintained at cathode potential (approximately -1300 V) to minimize dark noise.

3.4 – Solar tracking system

Within the BREWER software is an Ephemeris algorithm which calculates the azimuth and zenith angles of both the sun and the moon as seen from the current location. Data required for this calculation includes the geographic co-ordinates of the site, the GMT time, and GMT date. These angles are further processed by the software, and positioning commands are sent to the Zenith drive system and to the Azimuth tracker. The Azimuth Tracker is an all-weather positioning pedestal comprised of a weatherproof chassis which houses a stepper motor, drive electronics and a gearing mechanism. The tracker chassis is mounted on a Tripod assembly and is levelled by means of adjustments on each tripod leg. The positioning commands are input to a motor driver, which provides drive for a stepper motor. Automated Zenith positioning is performed by driving the Zenith prism with a stepper motor mounted on the front end of the foreoptics frame. In figure 3.7 the BREWER spectrophotometer Tracker / Tripod is showed.

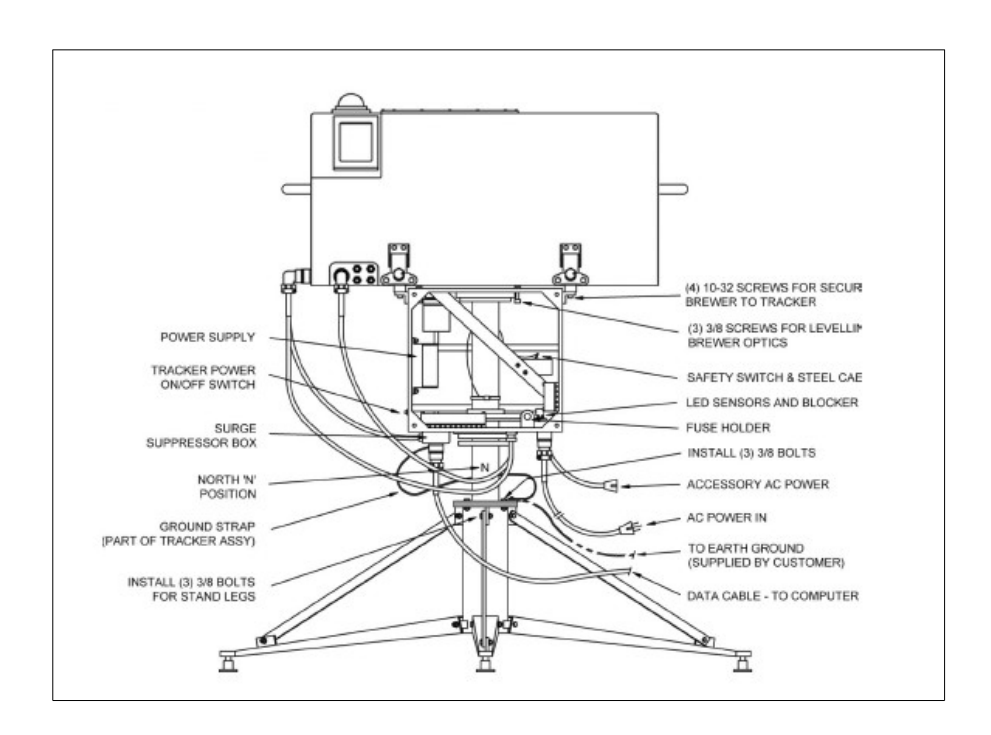


Figure 3.7 - BREWER Spectrophotometer Tracker / Tripod - (Courtesy of Kipp & Zonen).

3.5 – Personal Computer operating Software

The BREWER Spectrophotometer is operated by GWBasic software. This limits the amount of computer platforms suitable for operation.

Reliable PC platforms for BREWER operation are:

- DOS based computers
- Windows 3.1
- Windows 95
- Windows XP
- and in a number of cases also with Windows 98.

It is important for the computer to have at least one RS-232 serial communication port. For use with modern (64 bit) operating systems such as Windows Vista, Windows 7 and Windows 8, the WBasic software can be run using DosBox.

3.6 - Processing algorithm for total column ozone

The processing algorithm to infer total column ozone value from direct sun observations is showed in the following. To calculate total ozone values BREWER instruments require the determination of the weighted ozone absorption coefficient and the extra-terrestrial calibration (ETC) values as well as additional characteristics such as the temperature dependence of the instrument sensitivity. All these characteristics except for the ETC value can be determined from a set of tests on the instrument using standard sources of light. Regular tests made with the internal quartz halogen lamp make it possible to track the instrument response between the calibrations and ETC values.

In figure 3.8 the path geometry of sunlight passing through the ozone layer in the Earth's atmosphere is illustrated. If I_{λ} is the solar irradiance at wavelength λ measured at the Earth's surface by the instrument and $I_{0,\lambda}$ is the irradiance outside the Earth's atmosphere (extra-terrestrial value) at wavelength λ , the BREWER uses the irradiance at wavelength 310.1 nm, 313.5 nm, 316.8 nm and 320.1 to calculate the total column ozone using the following expression:

$$F + \Delta \beta \cdot m = F_0 - \Delta \alpha \cdot \Omega \cdot \mu \tag{3.1}$$

where

 Ω = total column ozone

m = the optical air mass of the whole atmosphere, equal to the ratio of the slant path of the beam through the whole atmosphere to the vertical path

 μ = the optical air mass of the ozone layer, equal to the ratio of the slant path of the beam through the ozone layer to the vertical path

 $F_0 = ETC$

F, $\Delta \alpha$, and $\Delta \beta$ are scalars formed respectively from the intensities I_i at the four wavelengths, the corresponding ozone absorption coefficients α_i and the Rayleigh scattering coefficients β_i .

$$F = \sum_{i=1}^{4} w_i \cdot \log(I_i), \quad \Delta \alpha = \sum_{i=1}^{4} w_i \cdot \alpha_i, \quad \Delta \beta = \sum_{i=1}^{4} w_i \cdot \beta_i$$

At the wavelengths 310.1 nm, 313.5 nm, 316.8 nm, and 320.0 nm the weighting coefficients (w_i) 1.0, -0.5, -2.2 and 1.7 have been chosen to minimize the effect of atmospheric SO₂ and small shifts in wavelength on the measurement and to suppress variations that change linearly with wavelength.

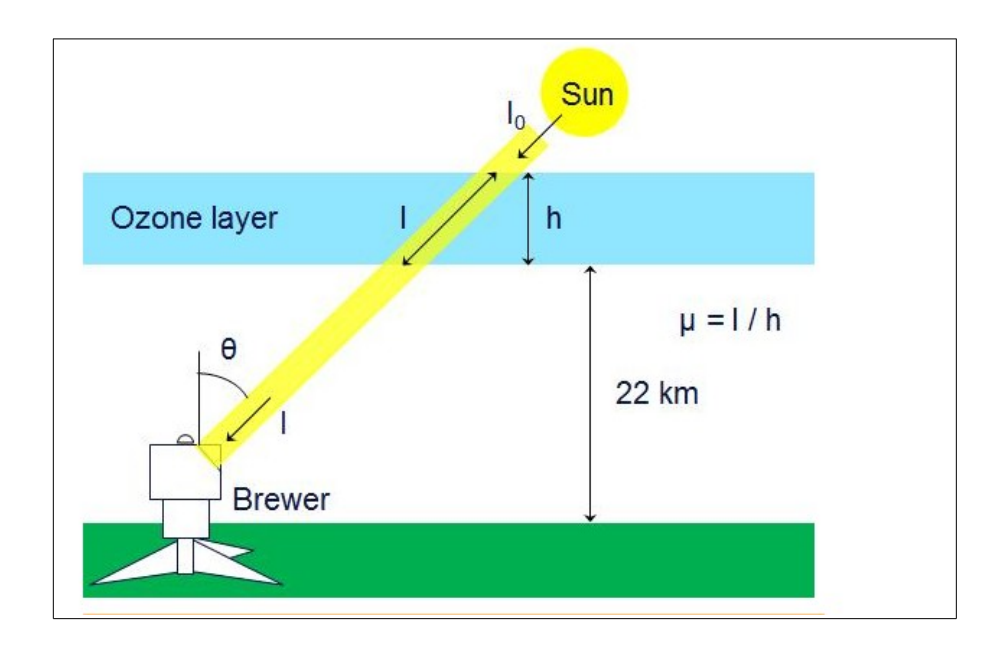


Figure 3.8 - Geometry for the path of sunlight passing through the ozone layer in the Earth's. - (Courtesy of Kipp & Zonen).

Once the values m, μ , $\Delta\alpha$, $\Delta\beta$, and F_0 are known, measuring F it is possible to determine the total ozone using (3.1).

$$\Omega = \frac{F_0 - F - \Delta\beta \cdot m}{\Delta\alpha \cdot \mu} \tag{3.2}$$

The BREWER calculates m and μ using the following equations:

$$m = \sec \theta = 1/\cos \theta \tag{3.3}$$

$$\mu(\theta) = \frac{1}{\sqrt{1 - \frac{(R+r)^2}{(R+h)^2} \sin^2 \theta}}$$
 (3.4)

where

 θ = zenith angle

R = the radius of the Earth

r = altitude of the station

h = altitude of the ozone layer

The BREWER algorithm assumes the ozone distribution is confined to a delta layer at a fixed altitude of 22 km above the station. Using a mean radius of the Earth of 6370 km and a null altitude for ground-based station a fixed value of 0.99656 for (R+r)/(R+h) is used.

The coefficient $\Delta\beta$ is determined from the Rayleigh scattering theory. The coefficient $\Delta\alpha$ is determined for each individual instrument from a set of tests, where the exact values of the instrument wavelengths are measured using a spectral lamp. The weighted ozone absorption coefficient $\Delta\alpha$ is calculated for these wavelengths using Bass-Paur ozone absorption coefficients. Absorption cross-sections of ozone have been measured over the range 230 nm to 350 nm, and for temperatures 200 K to 300 K, with improved photometric accuracy and spectral resolution.

F₀ values can be either transferred from the reference BREWER or determined directly by the Langley plot method, which allow to determine the Sun's irradiance at the top of the atmosphere by means of a ground-based sun photometer. The Langley plot method is applied to the BREWER reference triad established by Environment Canada at Toronto more than 20 years ago. The triad serves as a reference for travelling standard instruments that are used to calibrate BREWER spectrophotometers around the world. The long-term stability of BREWER network instruments is determined by the stability of the triad and the accuracy of the transfer of the calibration information from the triad to the travelling standard and from the travelling standard to the field instruments. Instrument properties change with time and the internal quartz halogen lamp is used to track these changes in instrument response. If the characteristics of the internal lamp remain settled, the measured intensity of the lamp signal reflects changes in the instrument sensitivity and can be used to adjust F_0 . In fact, the lamp characteristics are also changing with time, but these changes have little dependence on the wavelength. The weighted ratio used for ozone is insensitive to changes of intensity that are linear functions of the wavelength, and therefore is not very sensitive to the lamp degradation. The lamp characteristics are also monitored and lamps are replaced if changes of their characteristics are substantial. There were typically 2 to 8 measurements of the lamp intensity per day, known also as "standard lamp tests" (SL tests). The weighted intensity of lamp emission was averaged over a two-week period following the calibration and was used as a reference (L₀). The median value (L) of daily weighted averages from all SL tests within 2 weeks prior to and after a particular day was used as a reference for the instrument state for that day. The median value, instead of the mean, was used to avoid the influence from individual erroneous SL tests.

The adjusted ETC value

$$F_{0}^{'} = F_{0} - L_{0} + L \tag{3.5}$$

is used to calculate column ozone for that day.

The procedure described above reduces the effect of long-term changes of instrument characteristics on measured ozone. There are, however, short-term changes caused by internal instrument temperature (T) fluctuations. To compensate for these changes, the ETC value is further adjusted:

$$F_0' = F_0' + \tau \cdot (T - T_0) \tag{3.6}$$

where

T = instrument temperature

 T_0 = instrument temperature at the time of ozone calibration

τ = temperature coefficient, estimated from a set of SL tests taken typically as a part of the calibration procedure at a wide range of temperatures (0 °C to 30 °C)

To calculate the total ozone the BREWER effects direct sun (DS) measurements. Each DS measurement is based on a set of 5 sub-measurements, each of these is used to calculate a total ozone value. The average of these 5 values is reported as the ozone value for a DS measurement and their standard deviation is also reported as the measurement standard deviation (MSD). The MSD is used to determine the acceptability of each measurement. The normal acceptance criteria for DS measurements are MSD < 3 DU and μ < 3.5. The number of accepted DS measurements per day depends very much on season and weather and obviously on the schedule set.

3.7 - The Italian Air Force BREWER of Vigna di Valle

The Italian Air Force Technical Centre for Meteorology (CTM) is located 260 meters above mean sea level at the latitude of 42 ° 05 'North and the longitude of 12 ° 13' East. Overlooking the splendid Bracciano lake, the Centre is immersed in a characteristic landscape made up of hills vegetation and landscapes of enchanting charm.

The BREWER n° 065 is installed on the roof of the Meteorological Station (Figure 3.9). The BREWER of Vigna di Valle is one of the two instruments of the Air Force – Meteorological Service network (the other is installed in Sestola - Monte Cimone) and it starts ozone measurements since 1992.

The BREWER is part of the WMO network and the collected data are sent to the WMO World Ozone and Ultraviolet Data Centre (WOUDC) located in Toronto (Canada). Initially the BREWER, named n° 024, was a first generation instrument and was equipped with a single spectrometer. In 2006 the original instrument was modified and equipped with a double spectrometer assuming the present configuration.



Figure 3.9 – BREWER n° 065 of Vigna di Valle.

Chapter 4

COMPARISON BETWEEN SATELLITE AND GROUND TOTAL OZONE COLUMN MEASUREMENTS

4.1 – Objectives

In this chapter a comparison between collected total ozone column values at ground and on board satellite is made by means of a statistical analysis. In section 4.2 data collected by the Total Ozone Mapping Spectrometer (TOMS) on board satellite are compared with collected at ground by the BREWER spectrophotometer. In section 4.3 data collected by the Ozone Monitoring Instrument (OMI) on board satellite are compared with collected at ground by the BREWER spectrophotometer.

4.2 - Comparing TOMS - BREWER data

In this section the comparison between TOMS and BREWER total ozone column data collected in the period from January 1998 to January 2009 is showed. As mentioned before, the analysis was conducted on a statistical base. In the following we will assume the ground measurements as reference and we will investigate the matching between measurements collected on board satellite and the reference values. This choice is supported by the assumption that the algorithm used to derive satellite data have to be calibrated by means of ground measurements. The best first way to approach verification of continuous predictands is to produce a scatter plots, based on a number of total TOMS and BREWER data available in the analysed period (N=3071). Rather than being a verification measure, scatterplot is a means to explore the data and can thus provide a visual insight to the correspondence between the two variables distributions. An excellent feature is the possibility to appreciate at a glance potential outliers in either dataset. In figure 4.1 the scatterplot TOMS versus BREWER of total ozone column values is shown.

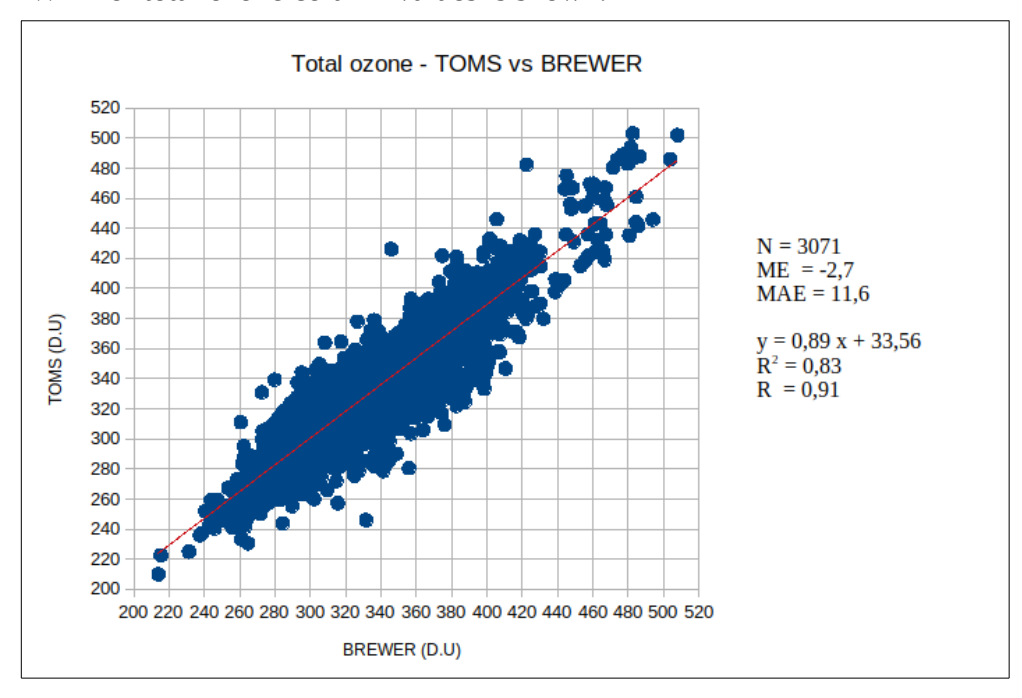


Figure 4.1 – TOMS vs BREWER scatterplot.

In an ideal situation, couple of TOMS and BREWER data should have the same value and the points should be lined on a 45 degree diagonal in a square scatterplot box. Looking at the scatterplot in figure 4.1 we can appreciate that the points seem to be well distributed around the diagonal and seem to indicate the absence of potential outliers. However scatterplot doesn't provide any concrete measures of accuracy, but only provides a visually descriptive method to reveal the presence of potential clustering, identification of potential outliers or curvature in the relationship between the two variables. In order to investigate how much TOMS and BREWER data data satisfy a linear relation, the correlation coefficient (R) and the determination coefficient (R²) were calculated.

We have:

$$Correlation coefficient(R) = \frac{\sum_{i=1}^{N} (Grd_i - \bar{Grd})^2 (Sat_i - \bar{Sat})^2}{\sqrt{\sum_{i=1}^{N} (Grd_i - \bar{Grd})^2 \sum_{i=1}^{N} (Sat_i - \bar{Sat})^2}}$$
(4.1)

where:

N = total number of measurements Grd_i = i-th ground observation Sat_i = i-th satellite observation Grd = mean value of Grd Sat = mean value od Grd

The correlation coefficient has two important properties. The first, it is bounded by -1 and 1. If R= -1 there is a perfect, negative linear association between the two variables. That is, the scatterplot consists of points all falling along one line, and that line has negative slope. Similarly if R=1 there is a perfect positive linear association. The second important property is that the square of the correlation coefficient (R²) specifies the proportion of the variability of one of the two variables that is linearly accounted for, or described by, the other. Notwithstanding a good value of the correlation coefficient give us some information about the linearity between two variable says nothing about the slope of the linear relationship between the two variables, except that it is not zero. To investigate if the angular coefficient of the linear relationship approach 45 degree a linear regression analysis was effected. Then a trend line was added to the scatterplot (red line) using the least squares method in order to identify the best line fit for the considered data set. The equation of the trend line and the determination coefficient value are reported in figure 4.1. R² value equal to 0.83 (R value equal to 0.91) indicates the positive linear association between TOMS and BREWER data. In addition, the trend line angular coefficient equal to 0,89 indicates the inclination of the best fit line approaching the slope of the diagonal. The final result is that TOMS and BREWER data are well linearly distributed around the diagonal.

In figure 4.2 and figure 4.3 the difference and the absolute difference (TOMS-BREWER) between satellite and ground data are respectively shown. The fist plot shows there isn't a net over estimation or under estimation of TOMS data respect BREWER data, that could led us to think at the presence of a bias. The second plot shows that after the first two years of measurements there was a reduction in the difference between TOMS and BREWER data until 2005 when the plot reveal an increase of the difference. An investigation was conducted and this increase was due to some BREWER spectrophotometers problems caused by a delay in the periodic instrument calibration.

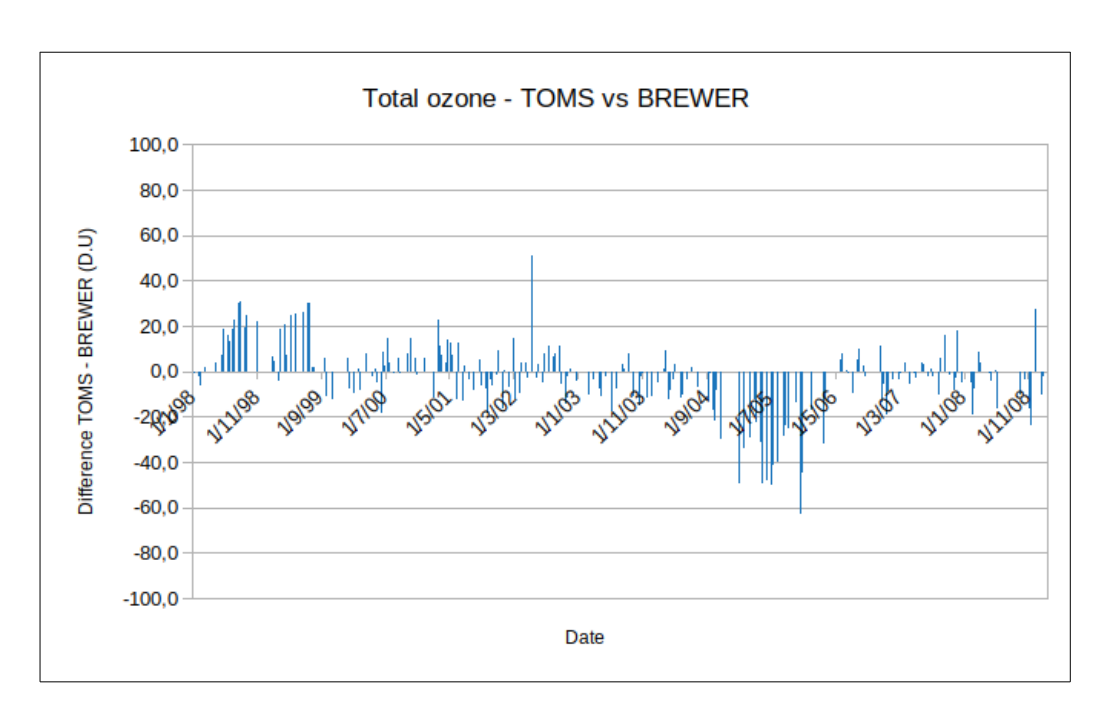


Figure 4.2 - Difference TOMS – BREWER.

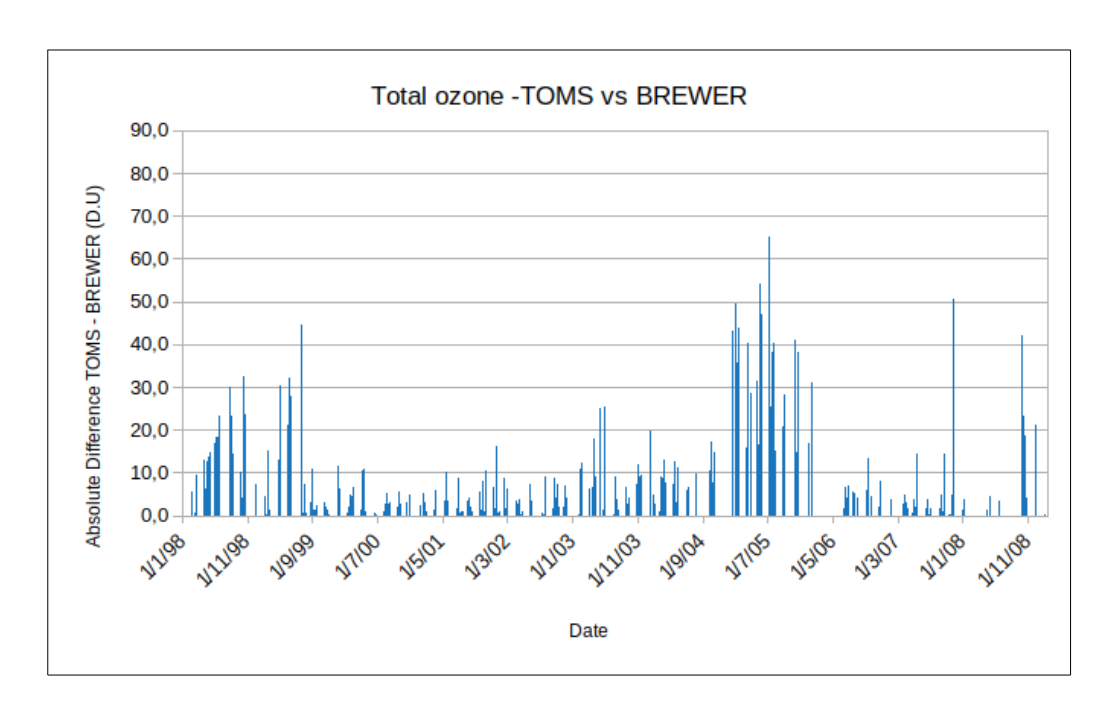


Figure 4.3 - Absolute Difference TOMS – BREWER.

To quantify the mean difference between the TOMS and BREWER data, the following statistical indexes are calculated:

$$Mean Error(ME) = \frac{\sum_{i=1}^{N} (Sat_i - Grd_i)}{N}$$
(4.2)

The ME represent the bias, it is the simplest and most familiar of scores and can provide very useful information on the local behaviour of a given parameter. The ME range is from negative infinity to infinity, and a perfect score is = 0. However, it is possible to reach a perfect score for a dataset with large errors, if there are compensating errors of a reverse sign. The ME is not an accuracy measure as it does not provide information of the magnitude of the errors.

Mean Absolute Error (MAE) =
$$\frac{\sum_{i=1}^{N} |Sat_{i} - Grd_{i}|}{N}$$
 (4.3)

The MAE is a simple measure to compensate for the potential positive and negative errors of the ME. The MAE range is from zero to infinity and, as with the ME, a perfect score is = 0. The MAE measures the average magnitude of the errors in a given dataset and therefore is a scalar measure of the accuracy. For this reason it is advisable to always view the ME and the MAE simultaneously.

The analysis result, computed from (4.2) and (4.3), are shown in table 4.A

N-total	ME	MAE	MEAN BREWER Value	MEAN TOMS Value
3071	-2,7	11,6	327,1	324,4

Table 4.A – TOMS vs BREWER statistical indexes analysis.

A negative ME value could indicate a negative bias, but the value lesser than 0,7% respect the mean BREWER value (equally to the TOMS value) confirms what is indicated by the difference plot that no bias is present. The small value of MAE shown there is not a significant compensation in the ME evaluation.

In figure 4.4 the graphical representation of monthly mean total column value versus time for BREWER and TOMS is shown. The plot shows again that after the first two years of measurements there was a reduction in the difference between TOMS and BREWER data until 2005 during which the plot reveal an increase of the difference.

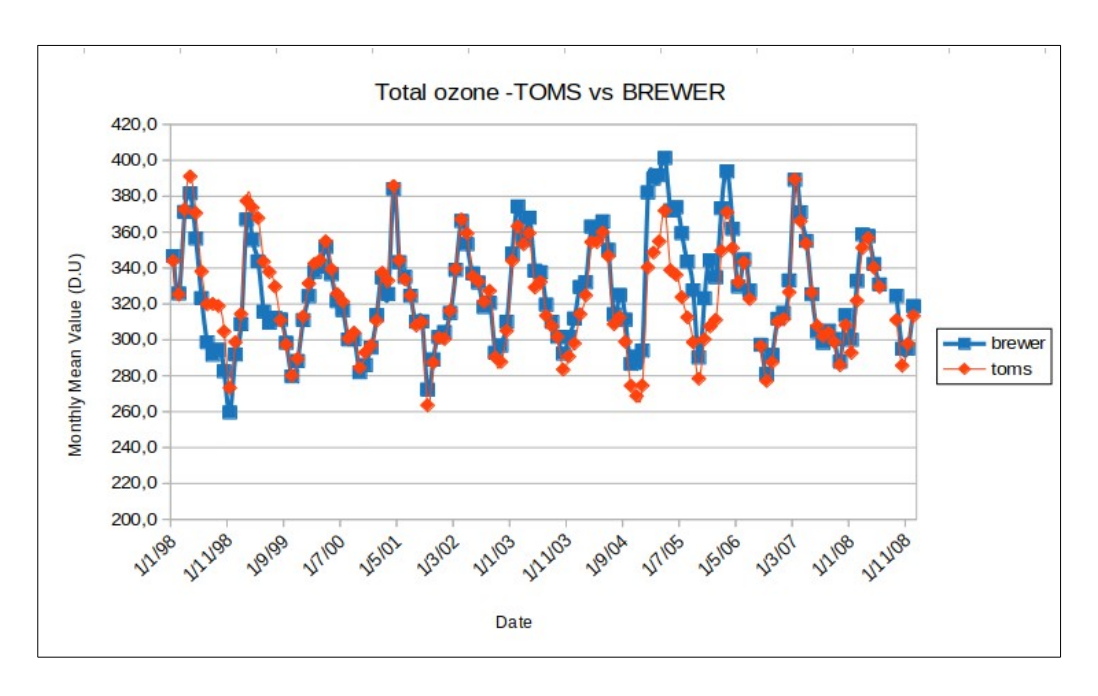


Figure 4.4 - Monthly mean total ozone column value versus time.

In figure 4.5 the difference (TOMS - BREWER) between satellite and ground data in function of total ozone is shown. The plot shows there aren't cluster or any kind of dependence on the ozone value.

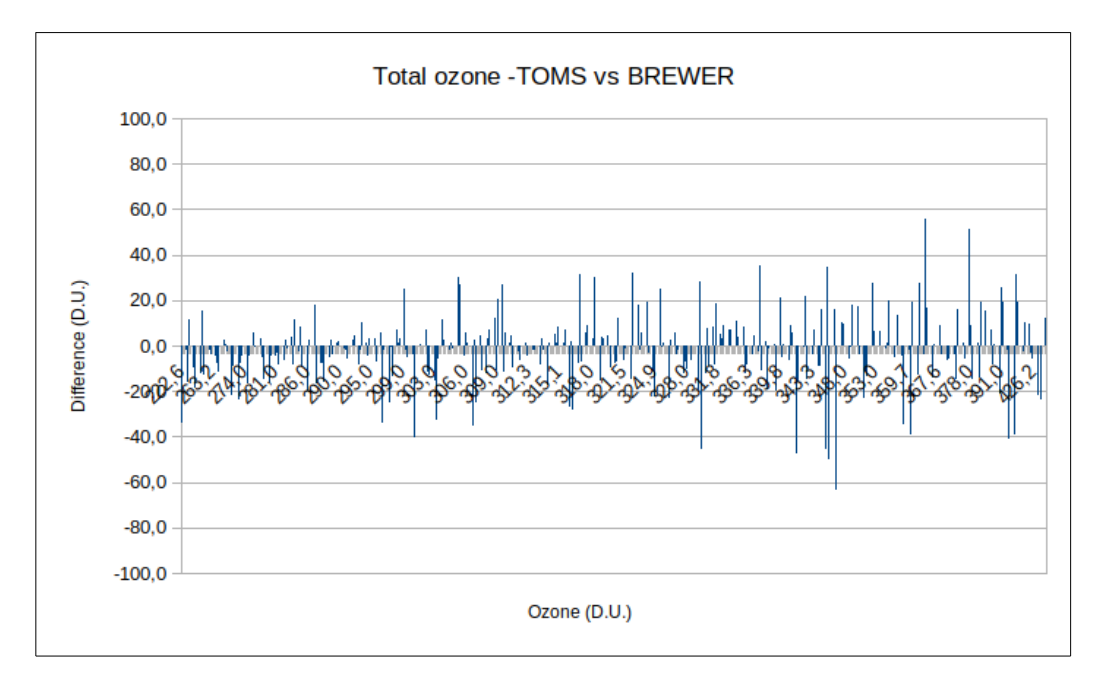


Figure 4.5 - Total ozone column value versus ozone value.

4.3 - Comparing OMI - BREWER data

In this section the comparison between OMI and BREWER total ozone column data collected in the period from September 2015 to September 2020 is showed. The analysis was conducted on a statistical base and also in this case the ground measurements are assumed as reference.

In figure 4.6 the scatterplot TOMS versus BREWER of total ozone column values is showed. The plot was produced using a number (N) of couple of TOMS and BREWER data available in the analysed period equal to 1143. The values seem to be well distributed around the diagonal except for some isolated points.

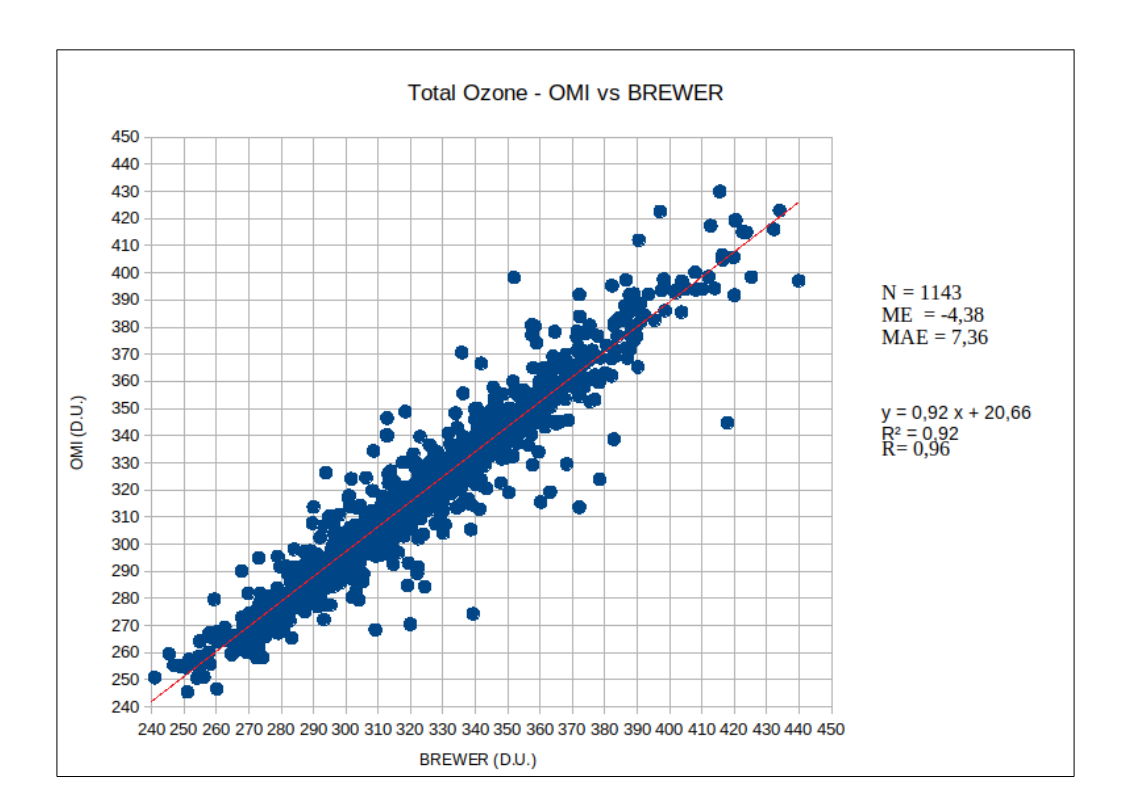


Figure 4.6 – OMI vs BREWER scatterplot.

The equation of the trend line and the determination coefficient value are reported in figure 4.6. R² value equal to 0,92 (R value equal to 0,96) indicates the positive linear association between OMI and BREWER data. The trend line angular coefficient equal to 0,92 indicates the inclination of the best fit line approach the inclination of the diagonal. The final result is that OMI and BREWER data are well linearly distributed around the diagonal.

In figure 4.7 and figure 4.8 the difference and the absolute difference (OMI-BREWER) between satellite and ground data are respectively shown. The fist plot suggest that could be the presence of a negative bias. The second plot shows that the difference between OMI and BREWER data has the same order in the considered period except in isolated days that could be related to the meteorological situation that was present and that will be subject of further investigation.

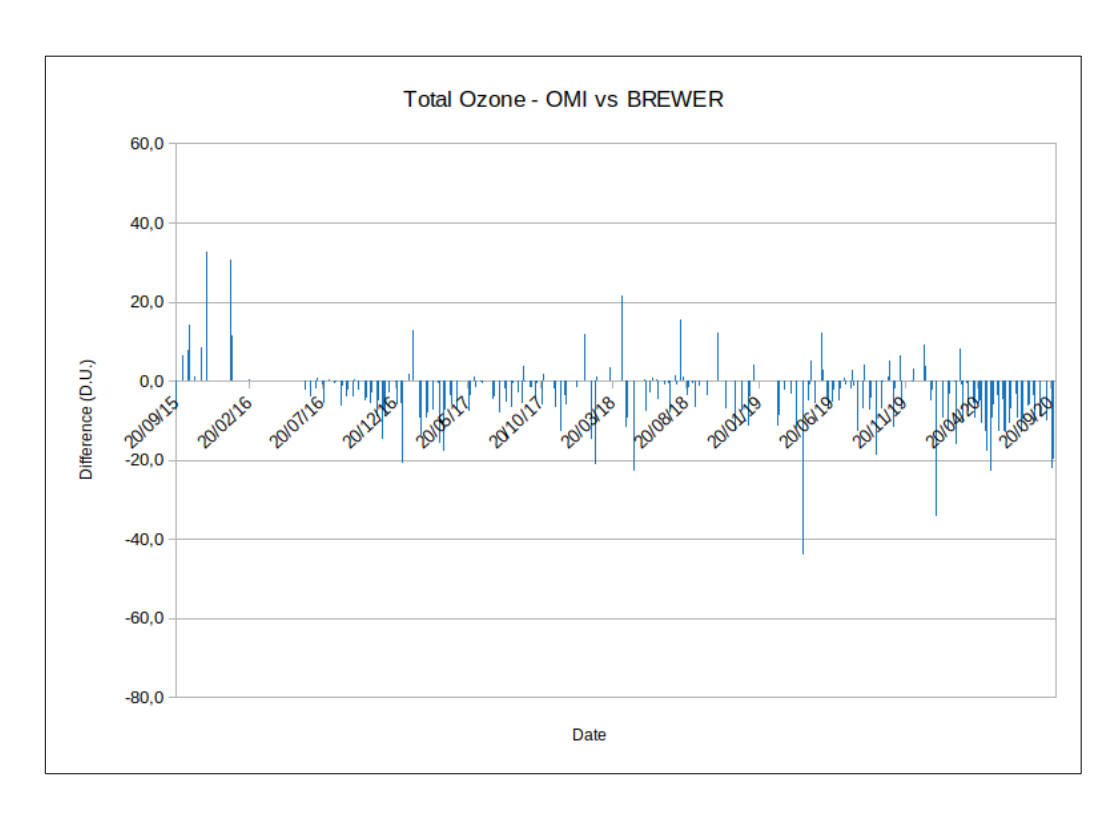


Figure 4.7 - Difference OMI – BREWER.

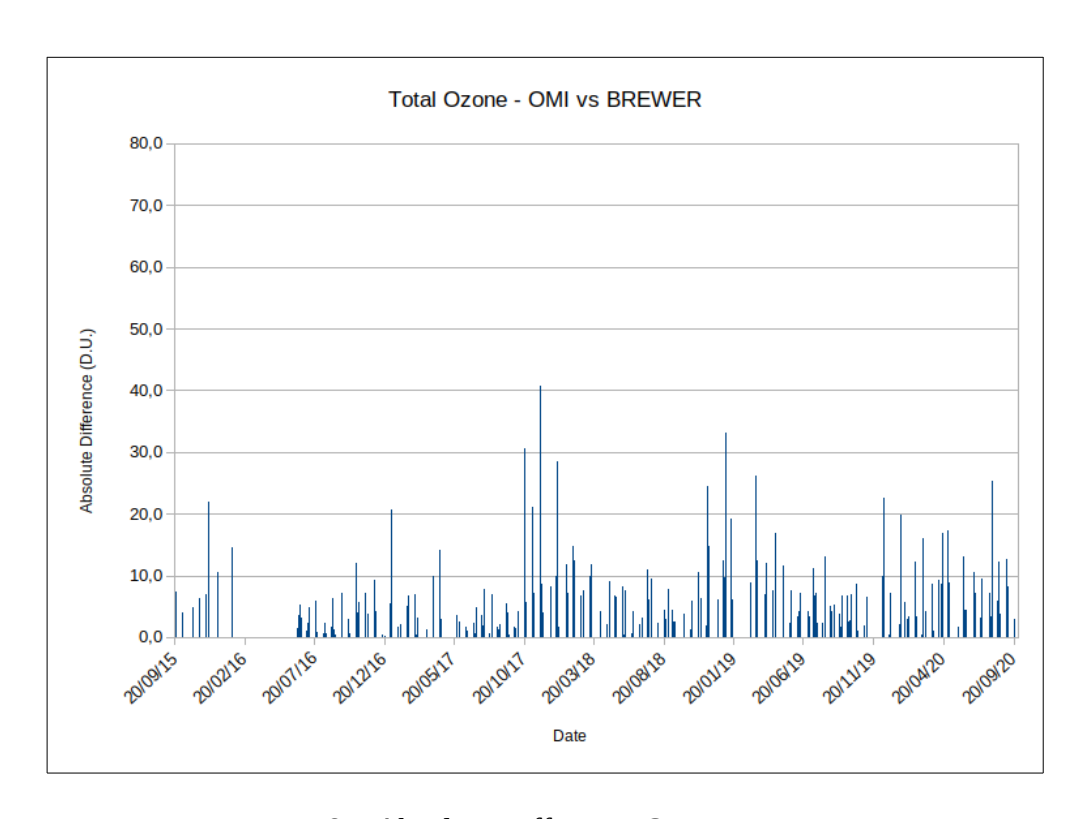


Figure 4.8 - Absolute Difference OMI – BREWER.

The statistical indexes, computed from (4.2) and (4.3), are shown in table 4.B.

N-total	ME	MAE	MEAN BREWER Value	MEAN OMI Value
1143	-4,38	7,36	321,1	316,8

Table 4.B – OMI vs BREWER statistical indexes analysis.

A negative ME value could indicate a negative bias, which confirm the visual result obtained from the plot analysis in figure 4.7, but the value lesser than 1,4% respect the mean BREWER value (equally to the OMI value) indicates that bias is no significant. The small value of MAE shows there is not a significant compensation in the ME evaluation.

In figure 4.9, the graphical representation of monthly mean total ozone value versus time for BREWER and OMI is shown. The plot shows the good agreement between satellite and ground data and confirms, except for the first year of measurement, the negative no significant bias.

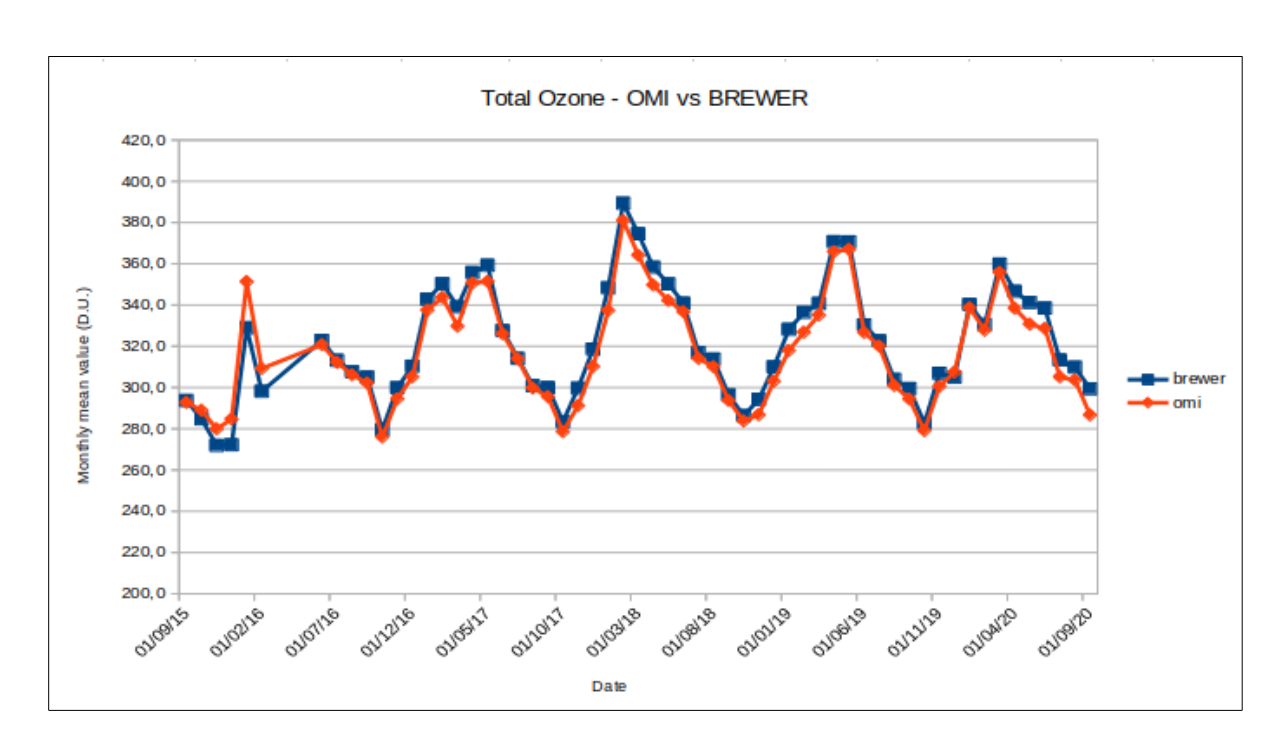


Figure 4.9 - Monthly mean total ozone column value versus time.

In figure 4.10 the difference (OMI - BREWER) between satellite and ground data in function of total ozone is shown. The plot shows there aren't cluster or any kind of dependence on the ozone value.

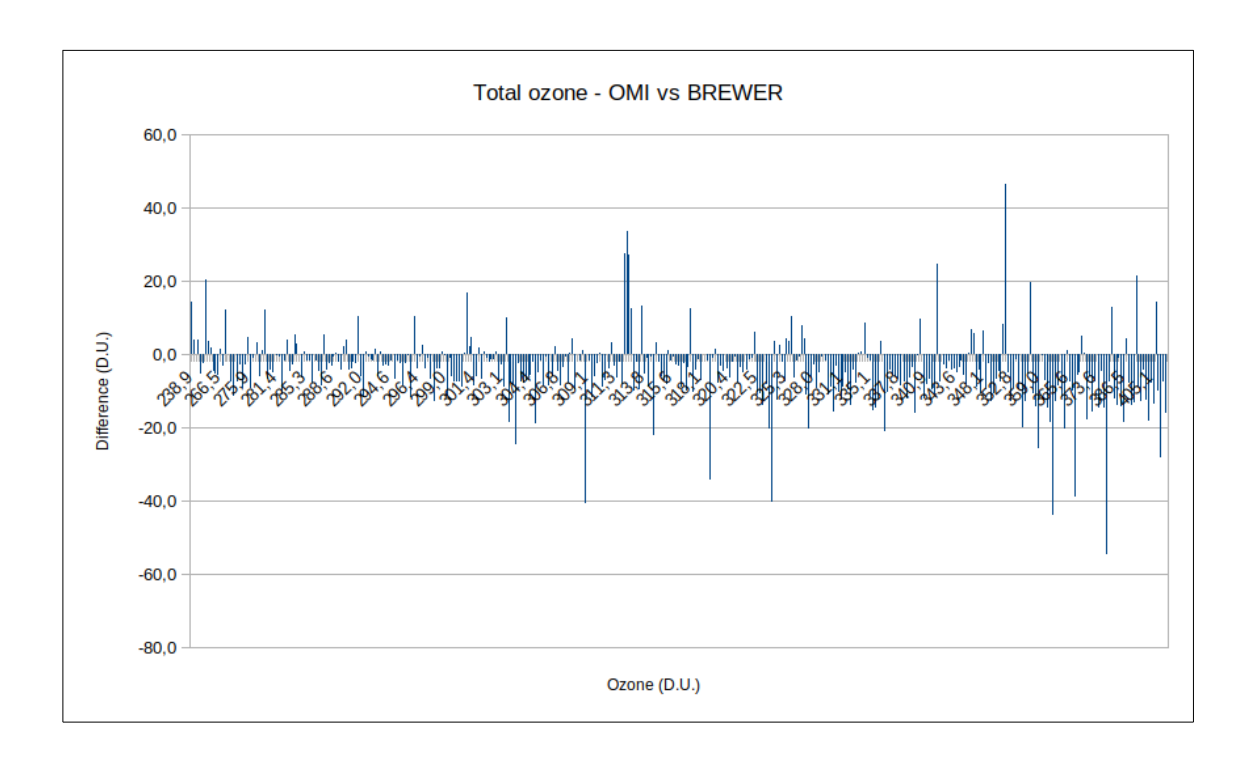


Figure 4.10 - Total ozone column value versus ozone value.

4.4 – Conclusions

In this study the results of the comparison between TOMS and BREWER total ozone column value and between OMI and BREWER total ozone column value were presented. Global analysis revealed a similar structures. In both cases the high values of the correlation coefficient and the slope values obtained by regression analysis suggest that satellite and ground measurements are in strong linear dependence. Concerning TOMS – BREWER comparison, the evaluation of Mean error and Mean absolute error indicates that no significant bias is present and the plots analysis reveal there are not cluster or any kind of the satellite algorithm dependence on the ozone value. Regarding OMI – BREWER comparison, the evaluation of Mean error, Mean absolute error and the plots analysis suggest the presence of a small negative bias, but the value is however are not significant. Also in the OMI -BREWER there are not cluster or any kind of the satellite algorithm dependence on the ozone value. In both comparisons between satellite and ground data there are some isolated outliers that seems to be associated to loss of calibration of the BREWER instruments or, in other cases, are probably due to the meteorological situation. These cases will be subject of future investigation.

In conclusion, even if TOMS and OMI algorithms differs the result obtained by a comparison with BREWER ground measurements are very similar and it is possible to conclude that satellite and ground measurement are in good agreement.

Bibliography

- Antón M., Koukouli M. E., Kroon M., McPeters R. D., Labow G. J., Balis D., and Serrano A.: Global validation of empirically corrected EP Total Ozone Mapping Spectrometer (TOMS) total ozone columns using Brewer and Dobson ground based measurements Journal of Geophysical Research, Vol. 115, D19305, doi:10.1029/2010JD014178, 2010.
- Bas A.M. and Paur R.J.: The ultraviolet cross-sections of ozone. Proceedings of the Quadrennial Ozone Symposium held in Halkidiki, Greece 3–7 September 1984 Zerefos C.S et al (eds.).
- Bhartia P.K.: OMI Algorithm Theoretical Basis Document, Volume II, OMI Ozone Products, ATBD-OMI-02, Version 2.0, August 2002.
- Dessler A. E.: The Chemistry and Physics of Stratospheric Ozone, 2000 International Geophysics Series Academic Press.
- Fiocco G.: Il Pianeta Terra, Lezioni di Fisica Terrestre.- Università degli Studi di Roma "La Sapienza", 1986.
- Fioletov V. E., Kerr J. B., McElroy C. T., Wardle D. I., Savastiouk V., and Grajnar T. S.: The Brewer reference triad Geophysical Research Letters, Vol. 32, L20805, doi:10.1029/2005GL024244, 2005.
- Fleagle R.G. and Businger J.A.: An Introduction to Atmospheric Physics, Second Edition. 1980 International Geophysics Series Academic Press.
- Gates D. M.: Biophysical Ecology Springer-Verlag, New York, 1980 edition.
- Holton J.R. et al: Stratosphere Troposphere exchange. Reviews of Geophysics, 33,4 /November 1995.
- Huffman R. E.: Atmospheric Ultraviolet Remote Sensing, 1992 International Geophysics Series Academic Press.
- Kipp & Zonen: Brewer MKIII Spectrophotometer Operator's Manual. Available at the following location: https://ozoneaq.gsfc.nasa.gov/media/docs/toms_algor.pdf
- Kroon M., Veefkind J. P., Sneep M., McPeters R.D., Bhartia P.K., and Levelt P. F: Comparing OMITOMS and OMI-DOAS total ozone column data. Journal of Geophysical Research, Vol. 113, D16S28, doi:10.1029/2007JD08798, 2008.
- Liou Kuo-Nan: An Introduction to Atmospheric Radiation, 2nd Ed. 2002 International Geophysics Series Academic Press.
- Mandel J.: The Statistical Analysis of Experimental Data Interscience Publishers, New York, 1964 edition.
- McCluney W.R.: Introduction to radiometry and photometry. 1994 Artec House, Boston-London.

- McElroy C.T. and Fogal P.F.: Ozone: From discovery to protection, 2008. Atmosphere-Ocean, 46:1, 1-13, DOI: 10.3137/ao.460101.
- Nurmi P.: Recommendations on the verification of local weather forecasts ECMWF Technical Memoranda, 2003 ECMWF library. Available at the following location: https://www.ecmwf.int/en/elibrary/11401-recommendations-verification-local-weather-forecasts
- Salby M.L.: Fundamentals of Atmospheric Physics, 1995 Vol. 61 in the International Geophysics Series Academic Press.
- Taylor J. R.: Introduzione all'analisi degli errori. 1999, Seconda edizione, ZANICHELLI.
- Twenty Questions and Answers about the Ozone Layer, 2018 Update. Component of the report of the Montreal Protocol titled Scientific Assessment of Ozone Depletion, 2018. Published online November 2019. Available at the following locations: http://ozone.unep.org/science/assessment/sap http://esrl.noaa.gov/csd/assessment/ozone/2018/
- Veefkind J. P., de Haan J. F., Brinksma E. J., Kroon M., and Levelt P. F.: Total Ozone From the Ozone Monitoring Instrument (OMI) Using the DOAS Technique IEEE Transactions on Geoscience and Remote Sensing, Vol. 44, N°. 5, May 2006
- Wellemeyer C.G., Bhartia P.K., Taylor S.L., Qin W., Ahn C.: Version 8 Total Ozone Mapping Spectrometer (TOMS) Algorithm, 2004. Available at the following location: https://ozoneag.gsfc.nasa.gov/media/docs/toms algor.pdf
- Wilks D.S.: Statistical Methods in the Atmospheric Sciences, 2nd Ed., 2006 International Geophysics Series Academic Press.